Aberrant N-glycosylation in pathogenic variants of adenosine deaminase 2 underlying human ADA2 deficiency

Lisa Ehlers[1] (ORCID: 0000-0001-8737-001X), Anneleen Hombrouck[1] (ORCID: 0009-0003-5236-6063), Marjon Wouters[1] (ORCID: 0000-0002-4675-1665), Bethany Pillay[1] (ORCID: 0000-0001-7964-544X), Selket Delafontaine[1] (ORCID: 0000-0002-8985-8155), Giorgia Bucciol[1] (ORCID: 0000-0001-5004-0738), Marco Baggio[1] (ORCID: 0000-0001-6708-9925), Mariia Dzhus[1] (ORCID: 0000-0002-2077-4295), Maarten Jacquemyn[2] (ORCID: 0000-0003-2626-4189), Lien De Somer[3,4] (ORCID: 0000-0002-8488-5090), Rik Schrijvers[5] (ORCID: 0000-0002-4261-6220), Steven Vanderschueren[6] (ORCID: 0000-0002-4003-5465), David Cassiman[7] (ORCID: 0000-0002-6154-0970), Marieluise Kirchner[8] (ORCID: 0000-0002-7049-534X), Philipp Mertins[8] (ORCID: 0000-0002-2245-528X), Tilmann Kallinich[9,10] (ORCID: 0000-0003-2404-9397), Dirk Daelemans[2] (ORCID: 0000-0001-7092-1153), Patrizia Agostinis[11] (ORCID: 0000-0003-1314-2115), Leen Moens[1] (ORCID: 0000-0002-5347-6526), Isabelle Meyts[1] (ORCID: 0000-0003-1214-0302)

Affiliations:

1 Department of Microbiology, Immunology and Transplantation, Laboratory for Inborn Errors of Immunity, KU Leuven, Leuven, Belgium

2 KU Leuven Department of Microbiology, Immunology and Transplantation, Laboratory of Virology and Chemotherapy, Rega Institute for Medical Research, Leuven, Belgium

3 Department of Pediatric Rheumatology, University Hospitals Leuven, Leuven, Belgium

4 Laboratory of Immunobiology, Department of Microbiology and Immunology, KU Leuven, Leuven, Belgium

5 Department of Microbiology, Immunology and Transplantation, Allergy and Clinical immunology Research group, KU Leuven, Leuven, Belgium

6 Department of General Internal Medicine, Research Department Microbiology, Immunology, and Transplantation, Laboratory of Clinical Infectious and Inflammatory Disorders, University Hospitals Leuven, Leuven, Belgium

7 Department of Gastroenterology-Hepatology and Metabolic Center, University Hospital Leuven, Leuven, Belgium

8 Core Unit Proteomics, Berlin Institute of Health at Charité - Universitätsmedizin Berlin and Max-Delbrück-Center for Molecular Medicine, Berlin, Germany

9 Department of Paediatric Pulmonology, Immunology and Critical Care Medicine, Charité – Universitätsmedizin Berlin, corporate member of Freie Universität Berlin and Humboldt-Universität zu Berlin, Berlin, Germany

10 Deutsches Rheuma-Forschungszentrum (DRFZ), an Institute of the Leibniz Association, Berlin, Germany

11 Cell Death Research & Therapy (CDRT) Lab, Department of Cellular & Molecular Medicine, Center for Cancer Biology, VIB-KU Leuven, Leuven, Belgium

Corresponding author:
Isabelle Meyts, Laboratory for Inborn Errors of Immunity and Department of Pediatrics UZ Leuven, Herestraat 49, 3000 Leuven, Belgium; Tel +32 16 343841; Fax +32 16 343842; isabelle.meyts@uzleuven.be

Summary

This study identifies a previously undescribed hypoglycosylated intracellular form of ADA2 in human monocyte-derived macrophages. Absence of this low-molecular-weight form is a key feature of human ADA2 deficiency (DADA2), suggesting a role for intracellular ADA2 in the pathogenesis of the disease.

Abstract

Pathogenic variants in *ADA2* underlie human deficiency of adenosine deaminase 2 (DADA2) and lead to impaired ADA2 protein secretion and reduced deaminase activity. Yet, the mechanisms driving the disease on a cellular level are poorly understood. Here, we report that *in vitro* differentiation of macrophages from DADA2 CD14+ monocytes partially restores protein expression of mutant ADA2. Healthy control macrophages express a high-molecular-weight (HMW) secreted form of ADA2 and a hypoglycosylated low-molecular-weight (LMW) intracellular protein. LMW-ADA2 is absent in DADA2 macrophages, suggesting differential glycosylation of mutant ADA2. In HEK293T cells transfected with pathogenic ADA2 variants, HMW-ADA2 accumulates intracellularly. Interactome analysis of the pathogenic variant p.R169Q revealed increased binding to proteins of the protein folding machinery compared with wild-type ADA2. Pathogenic ADA2 variants form intracellular protein aggregates and show increased degradation upon inhibition of the secretory pathway. In conclusion, we show aberrant N-glycosylation of ADA2 expressed in DADA2 macrophages for the first time and establish the absence of LMW-ADA2 as a characteristic of these ADA2-deficient cells.

Graphical abstract

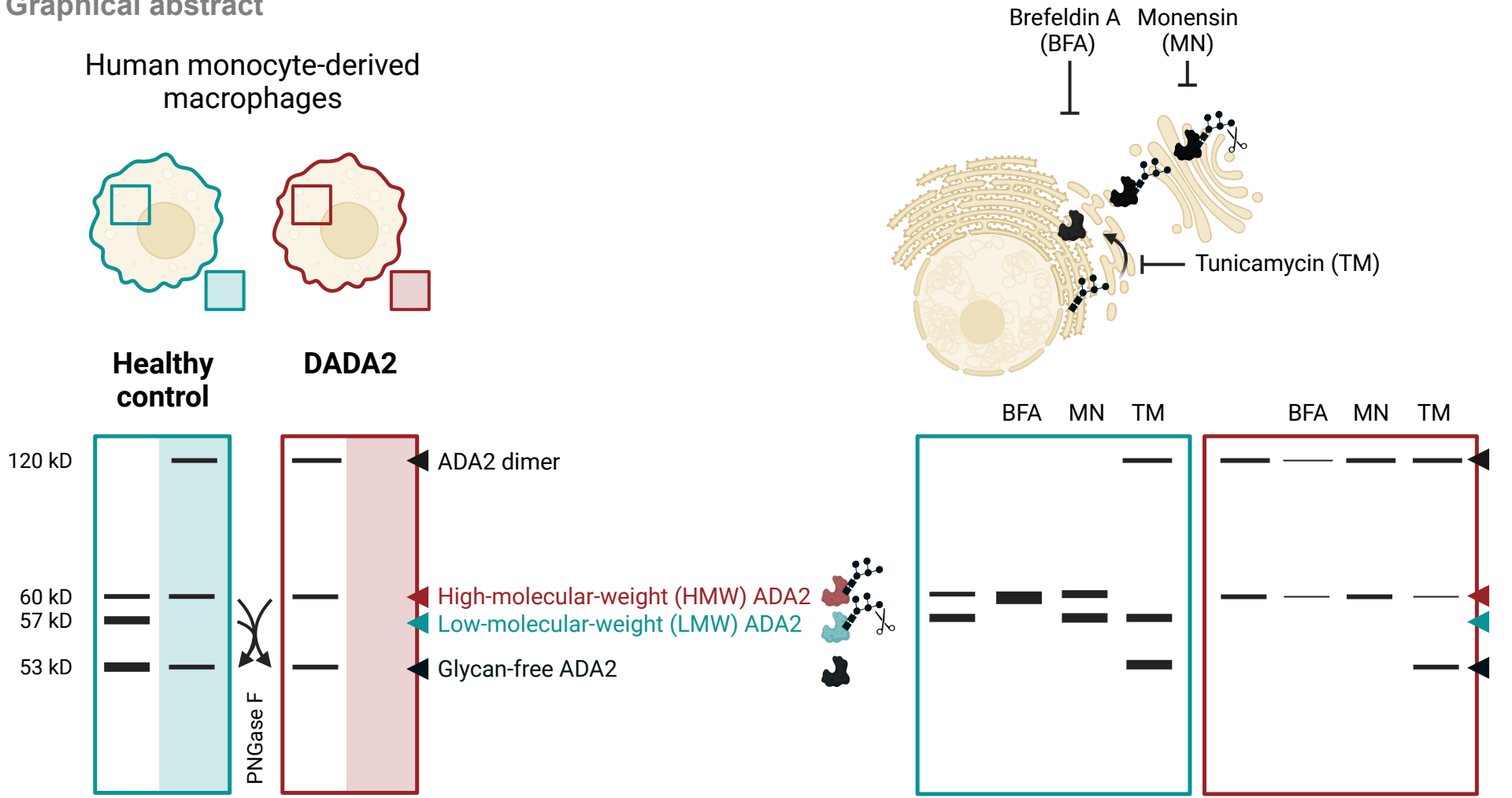

Introduction

Human deficiency of adenosine deaminase 2 (DADA2) is an inborn error of immunity caused by biallelic deleterious mutations in the *ADA2* gene (Zhou et al., 2014; Navon Elkan et al., 2014). The disease manifests with a diverse phenotype displaying features of both autoinflammation and immunodeficiency (Meyts and Aksentijevich, 2018). Almost 300 missense or predicted loss-of-function variants in *ADA2* are listed in the Genome Aggregation Database (gnomAD) (Karczewski et al., 2020). In the Infevers registry, 113 *ADA2* variants are classified as (likely) pathogenic (Infevers: an online database for autoinflammatory mutations.). Complete loss-of-function variants are more likely to cause bone marrow failure. Missense variants on the other hand are found in patients with a primarily vasculitis phenotype as well as in those presenting with cytopenias and hypogammaglobulinemia (Lee et al., 2020).

How mutations in *ADA2* give rise to this diverse phenotype, even in patients with identical genotypes, is not understood. Inflammatory symptoms of the disease typically respond well to TNF inhibitors (TNFi) (Deuitch et al., 2022). Insufficient resolution of bone marrow failure in response to this treatment however often necessitates hematopoietic stem cell transplantation and disease lethality still is 8% (Hashem et al., 2017). To develop improved treatment options, we require a better understanding of the pathomechanisms underlying the immunological and clinical phenotype of DADA2.

ADA2 is a glycoprotein with a signal peptide that mediates secretion of the protein via the endoplasmic reticulum (ER), and exhibits extracellular adenosine deaminase activity as a homodimer (Zavialov et al., 2010). The protein has four N-glycosylation sites and insufficient glycosylation leads to ER retention and intracellular aggregate formation of ADA2 transfected into HEK293T cells (Lee et al., 2018; Ito et al., 2022). Impaired protein secretion and absent serum ADA2 enzyme activity have been established as characteristics shared by the majority of pathogenic ADA2 variants (Chen et al., 2023). Mechanistic approaches to the pathophysiology of ADA2-deficient cells have therefore been based on impaired extracellular adenosine deamination driving inflammation (Carmona-Rivera et al., 2019; Dhanwani et al., 2020). This assumption fails to acknowledge the weak affinity of ADA2 for adenosine and the presence of functional ADA1 in DADA2 patients (Tarrant et al., 2022). Research into alternative functions of the ADA2 protein and DADA2-causing variants is therefore warranted. Biochemical characterization of pathogenic ADA2 variants has until now only been performed in a HEK293T overexpression system with supraphysiological intracellular levels of ADA2 while expression of the mutant protein has been shown to be minimal in DADA2 CD14+ monocytes (Chen et al., 2023; Greiner-Tollersrud et al., 2020). Disease-associated ADA2 variants have to date hardly been studied in their physiological milieu.

In this study, we analyze transport and modifications of endogenous ADA2 expressed in primary human immune cells from healthy donors and DADA2 patients in order to understand the characteristics of the intracellular protein and abnormalities due to pathogenic mutations. We provide evidence of distinct glycosylation patterns of ADA2 expressed in human macrophages and show that DADA2 macrophages are characterized by the absence of intracellular LMW-ADA2.

Results

In vitro macrophage differentiation partially restores ADA2 protein expression in DADA2 monocytes

We analyzed ADA2 protein expression and *ADA2* mRNA levels in peripheral blood leukocytes of ten DADA2 patients and three heterozygous carriers (**Table 1** and **Figure 1A**). CD14+ monocytes from DADA2 patients showed very low or absent ADA2 protein expression despite normal *ADA2* mRNA levels in patients with missense mutations (**Figure 1B** and **Figure S1A**). Upon macrophage differentiation, we observed an increase in mutant ADA2 protein expression in the patient cells while ADA2 protein expression was reduced in healthy control (HC) human monocyte-derived macrophages (HMDM) (**Figure 1C**). Successful differentiation of DADA2 HMDM was achieved both with granulocyte–macrophage colony-stimulating factor (GM-CSF) and macrophage colony-stimulating factor (M-CSF) (**Figure S1B**), which is in line with the reported restoration of macrophage differentiation under treatment with TNFi (Deuitch et al., 2022). Interestingly, western blotting of pathogenic ADA2 variants expressed in DADA2 HMDM revealed presence of only a high-molecular-weight (HMW) band of around 60 kD compared to HC HMDM displaying two bands at 60 and 57 kD, with the low-molecular-weight (LMW) band being more pronounced (**Figure 1C** and **Figure S1C**). A novel ADA2 variant serendipitously created in the process of generating an ADA2$^{-/-}$ Jurkat cell line showed the same phenotype (**Figure S1D**). The molecular weight of secreted wild-type (WT) ADA2 in the supernatant of HC HMDM corresponded to the intracellular HMW form – the only form expressed in DADA2 HMDM (**Figure 1C**). The secretion of HMW-ADA2 was confirmed in the monocytic cell lines U-937 and THP-1 (**Figure S1E**). HMDM from DADA2 patient P8 showed residual secretion of HMW-ADA2 that was equal in molecular weight to secreted WT ADA2 (**Figure S1F**). This HMW-form of ADA2 corresponded to the form detected in human serum (**Figure 1D**). Importantly, overexpression of tagged WT ADA2 and several confirmed pathogenic variants in HEK293T cells uniformly led to predominant intracellular expression of HMW-ADA2 (63 kD) which was equal in size to the secreted protein (**Figure 1E**). In line with our findings in DADA2 HMDM, intracellular LMW-ADA2 was absent after overexpression of mutant ADA2 in HEK293T cells (**Figure 1E**). Interestingly, this band was still present – albeit at lower levels – in the variants p.N127Q and p.W326R, two variants not found in DADA2 patients but created for the study of ADA2 glycosylation and dimerization, respectively (Lee et al., 2018; Zavialov et al., 2010). Collectively, we show that HC HMDM intracellularly express a form of ADA2 that is lower in molecular weight than the secreted protein. This LMW-form is absent in DADA2 HMDM while the secreted HMW-form is the form present intracellularly in DADA2 cells.

Human monocyte-derived macrophages intracellularly express a hypoglycosylated low-molecular-weight form of ADA2 that is absent in DADA2 macrophages

Differences in the molecular weight of a protein can be caused by posttranslational protein modifications and N-glycosylation of ADA2 has previously been confirmed (Zavialov et al., 2010; Greiner-Tollersrud et al., 2020; Ito et al., 2022). Therefore, we initially hypothesized that the LMW-form of ADA2 present only in cells expressing WT ADA2 corresponded to glycan-free ADA2. To test this, we performed glycan removal on lysates and supernatants containing ADA2 protein. Complete removal of N-glycans by Peptide-N-Glycosidase F (PNGase F) yielded a difference in

molecular weight of 7 kD between HMW-ADA2 and glycan-free ADA2 both overexpressed in HEK293T cells and endogenously expressed in the monocytic cell lines U-937 and THP-1 as well as HMDM (**Figure 2A+B**), revealing that LMW-ADA2 was in fact slightly bigger than glycan-free ADA2. Importantly, the anti-ADA2 antibody clone EPR25430-131 (#ab288296; abcam) was superior in detecting LMW-ADA2 but poorly detected glycan-free ADA2 (**Figure S2A**). Glycan removal by PNGase F cancelled out the differences in molecular weight between the LMW-form and the HMW-form in HMDM, yielding a single band of glycan-free ADA2 at 53 kD (**Figure 2B+C**). Hence, the distinct sizes of intracellular WT ADA2 (LMW) and secreted WT ADA2 or intracellular pathogenic ADA2 (both HMW) were due to differential protein glycosylation. Since glycan removal of LMW-ADA2 did not result in a smaller band than glycan removal of HMW-ADA2, these findings suggested partial glycosylation of the LMW-form. Of note, glycan removal yielded a smaller band of 53 kD in addition to the glycan-removed 56 kD protein for tagged WT ADA2 overexpressed in HEK293T cells that was absent for all tested pathogenic variants and did not appear after inhibition of N-glycosylation by tunicamycin (**Figure 2A**). As this band was absent after glycan removal of endogenous WT ADA2, its physiological relevance however is unclear.
Overall, we showed that the difference in size between HMW- and LMW-ADA2 is due to differential protein glycosylation.

Inhibition of N-glycosylation or ER glucosidases does not affect the glycosylation pattern of low-molecular-weight ADA2

In order to better characterize the glycosylation of endogenous ADA2, we inhibited N-glycosylation in HMDM and the monocytic cell lines U-937 and THP-1 by 24-hour treatment with tunicamycin. We found that this treatment only acted on the fully glycosylated, fainter HMW-band while LMW-ADA2 remained unchanged in size (**Figure 2D+E**). In accordance with previous findings (Ito et al., 2022), we showed that adenosine deaminase activity of ADA2 was preserved after glycan removal while treatment with tunicamycin reduced enzymatic activity. This was true for ADA2 overexpressed in HEK293T cells as well as endogenous ADA2 from HC HMDM (**Figure 2E+F**).
WT and mutant ADA2 were both sensitive to glycan removal by Endo H (**Figure 2G**), albeit incomplete compared to PNGase F (**Figure 2G**), hinting at the presence of high-mannose glycans in both LMW- and HMW-ADA2 expressed in HMDM. Treatment with castanospermine, an inhibitor of the ER glucosidases I and II, caused an additional increase in the size of HMW-ADA2 in both HC and DADA2 HMDM (**Figure 2H**). As seen previously upon incubation with tunicamycin, the LMW-form of ADA2, which is absent in DADA2 HMDM, was unaffected by this treatment (**Figure 2H**). We confirmed this finding in the three ADA2-expressing cell lines U-937, THP-1 and Jurkat (**Figure S2B**). Since the glycan pattern of LMW-ADA2 was unaffected by treatment with tunicamycin – an inhibitor of the initial step of N-glycosylation – we concluded that glycosylation of this form must have occurred prior to the treatment incubation period, suggesting high stability of LMW-ADA2. Accordingly, LMW-ADA2 was responsive to prolonged incubation with tunicamycin at a lower concentration (**Figure S2C**). The fact that the glycan structures of LMW-ADA2 were not subject to trimming by ER glucosidases further supports the hypothesis that glycan maturation of this form had already been completed before. Considering that HMW-ADA2 is responsive to both treatments, it is unlikely that LMW-ADA2 represents an intermediate – not yet fully glycosylated – form of "to be secreted" ADA2. We hypothesize that it might instead be generated by partial intracellular glycan trimming of the fully glycosylated form.
Since our data highlight the crucial role of N-glycosylation in ensuring successful folding and secretion of ADA2, we analyzed ADA2 expression in a patient with a mild form of *PMM2*-

congenital disorder of glycosylation. ADA2 expression and secretion in CD14+ monocytes and HMDM were equal to HC and no differences in molecular weight were noted, indicating unaffected ADA2 glycosylation (**Figure 2I**). This might however be due to the patient's mild phenotype and residual PMM2 activity. The patient also had normal serum ADA2 enzyme activity (**Figure 2I**).

Collectively, our findings suggest that the N-glycan structures of ADA2 contain high-mannose oligosaccharides and that the LMW-form is generated from HMW-ADA2 by intracellular glycan trimming.

The pathogenic ADA2 variant p.R169Q shows increased binding to proteins of the protein folding machinery

In order to elucidate whether differential glycosylation of HMW- and LMW-ADA2 might entail different protein functions, we performed immunoprecipitation followed by mass spectrometry (IP-MS) to analyze the interactome of WT ADA2 and the pathogenic variant p.R169Q transfected into HEK293T cells. p.R169Q displayed increased interaction with proteins involved in the ER quality control machinery for glycoproteins (**Figure 3A** and **Table S1**). Upon inhibition of N-glycosylation by tunicamycin, we observed a similar increase also for the WT protein (**Figure 3A** and **Table S1**), highlighting the importance of adequate N-glycosylation for successful folding and secretion of ADA2. Additionally, we observed an increase in lysosomal proteins in the ADA2 interactome after treatment with tunicamycin, suggesting autophagic degradation of non-glycosylated ADA2. Among the induced interactors were several proteins of the chaperone-mediated autophagy pathway, e.g. LAMP2 and HSPA13, and we verified the presence of a KFERQ-related motif (QKFVE, amino acids 274-278) in the sequence of ADA2 (Kirchner et al., 2019). IP-MS of HC and DADA2 HMDM did not yield any specific binders, which was possibly due to low protein abundance in the pull down of endogenous ADA2 (**Figure S3A**). Notably, IP preferentially pulled down the HMW-form of ADA2 (**Figure S3B+C**). The experiment consequently did not allow us to draw conclusions about the interactome and potential distinctive function of LMW-ADA2.

Given the increased binding of mutant ADA2 to the ER folding machinery, we verified whether pathogenic ADA2 variants induced an increased ER stress response. In line with previous reports (Chen et al., 2023), we observed that some pathogenic ADA2 variants caused signs of activation of an ER stress response, measured by increased levels of CHOP (*DDIT3*) and BiP (*HSPA5*) (**Figure S3D**). These differences were however no longer present after down-titrating the amount of transfected DNA to achieve near-physiological protein levels (**Figure 3B** and **Figure S3E**) and neither was there a difference in BiP expression in CD14+ monocytes from DADA2 patients compared to healthy controls (**Figure 3C**). Thus, our experiments revealed the interaction of the ADA2 variant p.R169Q overexpressed in HEK293T cells with mediators of the folding machinery and ER quality control despite no clear evidence of increased ER stress in the presence of pathogenic ADA2 variants. The interactome analyses were inconclusive regarding potential alternative functions of LMW-ADA2.

Impaired ADA2 secretion partially explains the intracellular predominance of fully glycosylated HMW-ADA2 in DADA2

We next sought to understand how protein glycosylation and trafficking differ between WT and mutant ADA2. We observed that fully glycosylated HMW-ADA2 persisted in cells transfected with the mutant p.R169Q after 24-hour incubation with tunicamycin (**Figure S3B**). Kinetics over 48

hours confirmed the increased presence of the glycosylated form of mutant ADA2 in comparison with WT ADA2 (**Figure 4A**). The same behavior was seen, albeit to different extents, in five additional pathogenic ADA2 variants (p.G47R, p.G47V, p.N127Q, p.T129P, p.P344L) (**Figure 4B**). Of note, p.N127Q and p.T129P are glycosylation site variants and therefore show a reduced molecular weight of the glycosylated HMW-band. To understand whether the persistence of glycosylated ADA2 was due to increased protein stability of mutant ADA2, we performed a cycloheximide chase assay which revealed higher levels of intracellular ADA2 protein expression in HEK293T cells transfected with mutant ADA2 compared to WT 24 hours after inhibition of protein synthesis (**Figure 4C**). Additionally, the assay showed that LMW-ADA2, only present in cells transfected with WT ADA2, was more stable than the HMW-form (**Figure 4C**).
Since ADA2 is a secreted protein, protein secretion must be taken into account when assessing the intracellular signal reduction in this assay over time. Impaired secretion has previously been established as a characteristic of pathogenic ADA2 variants (Navon Elkan et al., 2014; Chen et al., 2023). We confirmed the secretory defect in HMDM from our DADA2 cohort (**Figure 4D**). Overexpression in HEK293T cells reflected the endogenous behavior of the respective variants well (**Figure 4D**). While residual ADA2 enzyme activity largely correlated with preserved secretion, the catalytic domain variant p.N370K displayed absent deaminase activity despite comparatively high protein levels in the supernatant (**Figure 4D**). The partially preserved secretion of the variant p.G47R (Navon Elkan et al., 2014) was verified in HMDM from patient P8 who is homozygous for this variant (**Figure 4D**) and corresponded to higher serum ADA2 levels (**Figure 4D**) in the absence of serum deaminase activity (0.3 U/L).
Comparing the levels of increased ADA2 stability observed by cycloheximide chase assay with residual protein secretion, the variants p.T129P and p.R169Q that showed complete absence of secretion did indeed show the highest levels of intracellular ADA2 24 hours after inhibition of protein synthesis (**Figure 4C+D**). However, intracellular levels of the secreted mutant p.P344L were still higher compared to WT. By blocking the secretory pathway to impair secretion of WT ADA2, we confirmed that the secretory defect strongly contributed to the increased intracellular stability of mutant ADA2 (**Figure 4E+F**). Overall, we demonstrated increased intracellular stability of mutant ADA2 transfected into HEK293T cells, which was largely due to impaired protein secretion.

Pathogenic ADA2 variants form intracellular dimers

Upon overexpression of mutant ADA2 in HEK293T cells, we observed intracellular ADA2 dimer formation by western blot of whole cell lysates (**Figure 5A**). This behavior had previously been reported only for the ADA2 variant p.L351Q (Bowers et al., 2022). We observed that intracellular dimer formation largely correlated with impairment of ADA2 secretion although even pathogenic variants with residual secretion, p.G47R, p.N127Q and p.P344L, showed increased dimer formation compared to WT. Inhibition of N-glycosylation – but not of the secretory pathway – led to aggregate formation of WT ADA2 (**Figure 5B**), confirming the role of N-glycosylation in ensuring the structural integrity of ADA2 (Ito et al., 2022). We also detected intracellular dimers in DADA2 HMDM although the signal was weaker due to the strongly reduced protein expression of the pathogenic variants (**Figure 5C**). These findings indicate that impaired folding due to mutations or defective N-glycosylation promote intracellular aggregate formation of misfolded ADA2. To elucidate whether these aggregates actively disturb ADA2 secretion or form secondary to the impaired protein transport, we co-transfected HEK293T cells with varying amounts of WT and mutant ADA2. We found that the presence of the pathogenic variant p.R169Q caused dimer formation and impaired secretion of WT ADA2 overproportionally to the transfected ratios of WT

and mutant (**Figure 5D**), indicating that aggregate formation may indeed actively disturb ADA2 secretion. In line with this finding, we also observed that ADA2 serum protein levels of heterozygous carriers were in fact only 25% of healthy control (**Figure 5E**), while intracellular protein levels represented 75% of HC in CD14+ monocytes (**Figure 5F**). Thus, intracellular aggregate formation of pathogenic variants appears to contribute to impaired secretion of mutant ADA2.

Inhibitors of the secretory pathway differentially affect ADA2 variants

We showed that the secretory defect of mutant ADA2 was phenocopied by WT ADA2 upon inhibition of the secretory pathway by brefeldin A (**Figure 4F**). However, this treatment also caused increased degradation of the mutants p.G47V, p.T129P and p.R169Q (**Figure 4F**). To determine whether this effect was specific to brefeldin A, we also inhibited protein trafficking with monensin. Brefeldin A blocks protein transport from the ER to the Golgi apparatus while monensin inhibits trans Golgi transport (Fujiwara et al., 1988; Mollenhauer et al., 1990). Treatment with monensin also caused retention of WT ADA2 but protein levels of mutant ADA2 were unaffected (**Figure 6A**). Moreover, incubation with monensin led to an increase in the LMW-band present in cells overexpressing WT ADA2. The differential behavior in response to the secretory pathway inhibitors brefeldin A and monensin was confirmed in DADA2 HMDM (**Figure 6B**). Since treatment with brefeldin A caused increased protein degradation in several pathogenic ADA2 variants while resulting in intracellular accumulation of WT ADA2, we hypothesized that trafficking of mutant ADA2 differs from the WT protein. ER retention of mutant ADA2 has previously been shown in the HEK293T overexpression system (Lee et al., 2018; Chen et al., 2023). Strikingly, protein expression of pathogenic ADA2 variants in CD14+ monocytes from DADA2 patients is almost absent (**Figure 1B**). Considering the normal *ADA2* mRNA expression, this suggests rapid protein degradation of mutant ADA2, at least for the studied variants. Classically, misfolded secretory proteins are identified in the ER to be transferred to the cytosol for proteasome-mediated degradation, a process referred to as ER-associated degradation (Rubinsztein, 2006). Indeed, inhibition of the proteasome by delanzomib rescued the increased protein degradation of mutant ADA2 induced by treatment with brefeldin A (**Figure 6C**). Interestingly, p.R169Q degradation was also reduced by inhibiting lysosomal degradation with chloroquine (**Figure 6C**). This was in line with the increased interaction of misfolded ADA2 with lysosomal proteins identified by IP-MS. Lysosomal degradation of mutant ADA2 by autophagy might account for the differential response to treatment with monensin, a molecule that – besides its impact on Golgi transport – also inhibits autophagy (Boya et al., 2005). Importantly, inhibition of the proteasome or autophagy did not rescue increased protein degradation of mutant ADA2 in HMDM (**Figure 6D**), highlighting the limitations of protein transfection into HEK293T to model the mechanisms affecting pathogenic ADA2 variants endogenously expressed in primary patient cells. Overall, we showed that blocking ER to Golgi transport promotes protein degradation of mutant ADA2.

Discussion

In this study, we showed that pathogenic variants of ADA2 endogenously expressed in HMDM from DADA2 patients exhibit a glycosylation pattern that is characteristic of secreted WT ADA2 while lacking the LMW-form of ADA2 which is the predominant intracellular form in HC HMDM.

We reported the formation of intracellular protein aggregates in the presence of mutant ADA2 and increased protein degradation of pathogenic variants upon inhibition of the secretory pathway.
The importance of N-glycosylation in trafficking and function of ADA2 has previously been established (Lee et al., 2018; Ito et al., 2022). Yet, the behavior of mutant ADA2 on the cellular level has to date only been examined in overexpression systems of cells that do not express the protein endogenously (Chen et al., 2023; Bowers et al., 2022; Ito et al., 2022). Expression of glycosyltransferases and glycosidases and therefore glycosylation patterns of individual proteins show striking variation even between different immune cell populations (Daniels et al., 2002). It is therefore essential to understand the behavior of ADA2 in the context of the patients' primary cells. In our cohort of ten DADA2 patients, we identified the intracellular predominance of fully glycosylated HMW-ADA2 in the absence of LMW-ADA2 as a feature that was shared by all missense variants, independently of the patients' clinical phenotype. Differential patterns of glycosylation of the same protein being associated with distinctive protein functions have previously been described: IL-24 is a signal peptide-containing glycoprotein that is secreted via the ER. Recently, a partially glycosylated cytosolic form of the protein has been shown to mediate protein kinase R activation independently of its extracellular function (Davidson et al., 2022). The predominance of the partially glycosylated LMW-form of ADA2 in HC HMDM raises the question of whether, in a similar way, this form might differ in function from fully glycosylated secreted ADA2. In fact, the true function of ADA2 has repeatedly been subject to discussion for several reasons: (i.) Pathogenic ADA2 variants display a wide spectrum of residual adenosine deaminase function that cannot be clearly correlated with disease severity (Jee et al., 2021). (ii.) ADA2 has evolved towards lower affinity to adenosine in higher species (Zavialov et al., 2010). (iii.) ADA1 exhibits superior adenosine deaminase activity (Km of 20-50 μM vs. 2-3 mM for ADA2) and extracellular ADA1 bound to CD26 should compensate for the absence of ADA2 at physiological levels of adenosine (Tarrant et al., 2022). Yet, the majority of studies proposing possible pathomechanisms underlying the immunological phenotype of DADA2 rely on the role of ADA2 as an extracellular adenosine deaminase (Dhanwani et al., 2020; Carmona-Rivera et al., 2019). In contrast, Greiner-Tollersrud and colleagues introduced the possibility of an intracellular function of ADA2 as a lysosomal DNase (Greiner-Tollersrud et al., 2020). The authors characterized the glycan structures of ADA2 isolated from porcine brain and identified a high mannose-6-phosphate content, indicating targeting of ADA2 to the lysosome. Indeed, they showed an overlap between the glycosylation pattern of ADA2 with several known lysosomal proteins. We showed that the glycan structures of LMW- and HMW-ADA2 expressed in HMDM were sensitive to glycan removal by Endo H, suggesting the presence of high-mannose oligosaccharides (Kim and Leahy, 2013). This would be in line with a potential lysosomal localization of ADA2. Whether the predominant intracellular LMW-form of ADA2 that we detected in HMDM represents this lysosomal protein cannot be conclusively established from our data. Due to insufficient pull-down of LMW-ADA2 by immunoprecipitation, we could not elucidate its interactome and approach its potential function in this way. In the HEK293T model system, transfected ADA2 was predominantly expressed as the HMW-form that was equal to secreted ADA2 in these cells, highlighting the limitations of this system to understand the behavior of endogenous ADA2. Discrepancies between the two systems are also evident from the fact that ADA2 in whole cell lysates from transfected HEK293T cells was equally sensitive to glycan removal by PNGase F or Endo H (Ito et al., 2022), while we observed some residual glycan structures upon Endo H treatment of ADA2 in lysates from HMDM (**Figure 2G**). In HMDM, we did not observe the rescue of brefeldin A-induced degradation of mutant ADA2 by inhibition of proteasomal or lysosomal degradation shown in HEK293T cells. It is possible that in these cells the two protein degradation pathways mutually compensate for the inhibition of the other.

Another limitation of the relevance of macrophage LMW-ADA2 in the pathogenesis of DADA2 is that in primary CD14+ monocytes, the cells with the highest endogenous expression of ADA2, differentially glycosylated forms of ADA2 cannot be clearly distinguished (**Figure 1B**). Moreover, patient cells show complete absence of mutant ADA2, implying that mutations in the *ADA2* gene might manifest differently on a cellular level depending on the expressing cell.

This needs to be taken into account when examining the potential induction of ER stress by pathogenic variants of ADA2. Intracellular retention of ADA2 has only been reported after overexpression in HEK293T cells (Navon Elkan et al., 2014; Chen et al., 2023). While primary monocytic cells also show impaired secretion of mutant ADA2, intracellular protein levels are very low in HMDM and close to absent in CD14+ monocytes. In our cohort of DADA2 patients, we did not observe an increased ER stress response in CD14+ monocytes. This was in line with single-cell RNA-sequencing data reported by Watanabe et al. that showed downregulation of eIF2 signaling – a main pathway of the integrated stress response (Watanabe et al., 2021; Pakos-Zebrucka et al., 2016).

Although we could not verify that the presence of misfolded mutant ADA2 contributes to the pathophysiology of the disease by induction of an unfolded protein response, our data still highlight the need for a better understanding of the folding and trafficking of WT and mutant ADA2. We verified that the presence of pathogenic ADA2 variants as well as inhibition of N-glycosylation provoked the formation of intracellular protein aggregates, thereby confirming and broadening previous reports (Ito et al., 2022; Bowers et al., 2022). In addition, we showed that aggregate formation even occurs after co-transfection in the presence of the wild-type protein. These findings provide a possible basis for heterozygous carriers presenting with clinical symptoms and highlight the need for an in-depth understanding of the intracellular pathophysiology of DADA2. Serum ADA2 enzyme activity currently represents the diagnostic gold standard for DADA2. Assuming an intracellular function of the protein, it is possible that this strategy misses a proportion of patients. In this article, we introduced the absence of LMW-ADA2 as a new characteristic of pathogenic ADA2 variants that was verified for all pathogenic missense and deletion mutations included in this study. This suggests a possible role of this form as a biomarker in DADA2, which would need to be established in a larger set of pathogenic and benign ADA2 variants.

Protein misfolding represents a major aspect in the pathogenesis of mendelian diseases. In recent years, we have learned that for some proteins, function can be rescued to a certain extent by pharmaceutically modifying protein folding. Biallelic mutations in *CFTR* cause cystic fibrosis, one of the most common mendelian diseases. The most common pathogenic variant p.ΔF508 is almost entirely degraded via the ER-associated degradation pathway (Pankow et al., 2015). CFTR correctors have been shown to promote folding of the mutant protein and thereby partially restore the function of the channel to clinically relevant levels (Fiedorczuk and Chen, 2022). In order to envision similar approaches to treat DADA2, a thorough understanding of ADA2 transport and function would be crucial. The fact that ADA2 behaves differently depending on the expressing cell further complicates this approach. Until now, monocytes as the main producers of endogenous ADA2 have received the most attention in deciphering the pathophysiology of the disease. Considering the role of glycosylation in protein folding and the potential impact of this modification on protein function, we cannot exclude that the main ADA2 function might vary even between different immune cells. This might also account for the diverse clinical phenotype of the disease and the varying involvement of different immune cell populations. The large number of pathogenic variants and their diversity with respect to biochemical characteristics are additional factors contributing to the difficulties in delineating one all-encompassing pathomechanism that would explain the disease in its complexity.

In conclusion, we demonstrate for the first time differential N-glycosylation of pathogenic ADA2 in patient-derived macrophages. We establish LMW-ADA2 as a hypoglycosylated non-secreted form of ADA2 in healthy controls, a form that is absent in DADA2. Further studies will be needed to confirm the functional relevance of these results in the pathogenesis of the disease.

Materials and methods

Human subjects

The patients and heterozygous carriers were treated at University Hospitals Leuven and their parents were included as heterozygous carriers. Healthy donors were recruited at University Hospitals Leuven and KU Leuven. This study was performed in accordance with the ethical standards as laid down in the 1964 Declaration of Helsinki and its later amendments and was approved by the Ethics Committee for Research of Leuven University Hospitals (project numbers S63077, S63807).

Sanger sequencing

Genomic DNA samples were prepared from heparinized peripheral blood or $1x10^6$ Jurkat cells following the instructions of the QIAamp DNA Blood Mini kit (#51104; QIAGEN). Primers were designed with the help of Oligo Primer Analysis Software version 7 (Molecular Biology Insights). ADA2-specific gDNA amplification was performed using Platinum™ SuperFi™ PCR Master Mix (#12358010; Thermo Fisher Scientific). PCR products were purified using the QIAquick PCR purification kit (#28106; QIAGEN). Sanger sequencing was performed on an ABI 3730 XL Genetic Analyzer (Applied Biosystems) at LGC Genomics (Berlin, Germany). Sequencing data were analysed using Chromas 2.6.5 (http://www.technelysium.com.au).

Cell culture

Peripheral blood mononuclear cells (PBMCs) were isolated by density gradient centrifugation using Lymphoprep™ (#1114546; PROGEN) in SepMate™ isolation tubes (#85450; STEMCELL Technologies) according to the manufacturer's instructions. Prior to monocyte isolation, the final centrifugation step was performed at 300xg for 10 minutes at 4°C. CD14+ monocytes were isolated magnetically by positive selection using human CD14 MicroBeads (#130-050-201; Miltenyi Biotec) on LS columns (#130-042-401; Miltenyi Biotec) according to the manufacturer's protocol. The cells were eluted into complete medium (RPMI 1640 medium (#61870044; Gibco) supplemented with 10% fetal calf serum (FCS) (#S181BH-500, Biowest) and 1% penicillin-streptomycin (#15140122; Gibco). Purity > 97% of CD14+ monocytes after magnetic sorting was verified by flow cytometry (anti-CD14-FITC clone MφP9, 1:40, #345784; BD Biosciences). For macrophage differentiation, $3x10^5$ CD14+ monocytes were seeded in a 12-well plate in 1 mL complete medium containing 20 ng/mL GM-CSF (#300-03; Peprotech) or 50 ng/mL M-CSF (#300-25; Peprotech). The cells were differentiated for ten days, with medium changes every three days. U-937, THP-1 and Jurkat cells (all purchased from ATCC) were cultured in complete RPMI medium. HEK293T cells (ATCC) were cultured in DMEM supplemented with 10% FCS and 1% penicillin-streptomycin. For transfection, the cells were seeded in medium containing no antibiotics.
Inhibition of the secretory pathway was achieved by 24-hour incubation with 1 μg/mL brefeldin A (#00-4506-51; Thermo Fisher Scientific) or 2 μg/mL monensin (GolgiStop™, #554724, BD

Biosciences). For analysis of N-glycosylation and glycan trimming, the cells were incubated with tunicamycin (#T7765; Sigma-Aldrich) at 2.5 μg/mL (HEK293T cells) or 5 μg/mL (HMDM) and castanospermine (#BML-S107-0100; Enzo Life Sciences) at 100 μg/mL for 24h. Monocytes were treated with 1 μg/mL tunicamycin for 24h for ER stress induction. Cells were treated with 50 μM chloroquine (#C6628; Sigma-Aldrich) for 24h to inhibit autophagy. Proteasome inhibition was achieved by 24-hour incubation with 200 nM delanzomib (#S1157; Selleck Chemicals GmbH).

Microscopy

HMDM were differentiated with GM-CSF or M-CSF for 10 days in a 12-well plate as described above. Cell morphology was evaluated in the culture plate by brightfield microscopy on an EVOS M7000 Microscope Imaging System (#AMF7000; Invitrogen) using the 20x objective.

Transfection

The plasmid expressing myc-DDK-tagged wild-type ADA2 (transcript variant 3, NM_001282225) was purchased from OriGene Technologies (#RC238645). Pathogenic ADA2 variants were created by site-directed mutagenesis using the Q5® Site-Directed Mutagenesis Kit (#E0554; New England Biolabs) according to the manufacturer's instructions. Stable competent E. coli (#C3040H, New England Biolabs) were transformed with the generated constructs. Plasmid DNA was purified with the help of the QIAprep Spin Miniprep Kit (#27104, QIAGEN). Successful mutagenesis was verified by Sanger sequencing (LGC Genomics). HEK293T cells were seeded at $5x10^4$ cells/well in 1 mL in a 24-well plate or $2.5x10^5$ cells/well in 2 mL in a 6-well plate 24h prior to transfection. The cells were transfected with 5 ng and 25 ng plasmid DNA, respectively, using Lipofectamine™ 2000 Transfection Reagent (#11668019; Invitrogen) according to the manufacturer's instructions. The medium was changed after 24h. Cells and supernatants were collected 48h after transfection.

Generation of ADA2$^{-/-}$ cell lines by CRISPR/Cas9

Single-guide RNAs targeting ADA2 from the human CRISPR Brunello library (#73179; addgene) (Doench et al., 2016) were cloned into the lentiCRISPRv2 puro plasmid. lentiCRISPRv2 puro was a gift from Brett Stringer (plasmid #98290; addgene; http://n2t.net/addgene:98290; RRID:Addgene_98290). Jurkat cells were transfected by electroporation using the Neon™ Transfection System (#MPK5000; Thermo Fisher Scientific) according to the manufacturer's instructions: $2x10^5$ cells were resuspended in Resuspension Buffer R and mixed with 1 μg plasmid DNA. Electroporation was achieved with the following conditions: 1325V, 10ms, 3 pulses. After electroporation, the cells were directly transferred into 500 μL prewarmed complete RPMI 1640 medium. On day 1 after transfection, puromycin (#ant-pr-1; InvivoGen) was added at a final concentration of 1 μg/mL. After 36h, cells were seeded at 1 cell/well in 100 μL RPMI 1640 medium supplemented with 20% FCS in a round bottom 96-well plate. After 14 days, the clones were screened for knock out of ADA2 by western blot.

Immunoblotting

Adherent cells were detached with trypsin-EDTA (0.05%) (#25300062; Gibco) for 5 minutes at 37°C and the reaction was blocked by addition of complete medium. Cells were pelleted by centrifugation at 400xg for 5 minutes at 4°C. Whole cell lysates were obtained by lysing $1x10^6$ cells in 25 μL RIPA buffer (150 mM NaCl, 1% Triton X-100, 0.5% sodium deoxycholate, 0.1% SDS,

pH 8.0) or NP-40 lysis buffer (150 mM NaCl, 50 mM Tris-HCl, 1% NP-40, pH 7.4) containing protease inhibitor (#78429; Thermo Fisher Scientific) for 30 minutes on ice, followed by centrifugation at 13,500xg for 20 minutes at 4°C.
To collect supernatants, cells were cultured in serum-free medium for 24h. For immunoblotting, supernatants were concentrated by added 1200 µL ice-cold acetone to 300 µL supernatant and overnight storage at -20°C. Supernatant proteins were then precipitated by centrifugation at 15,000xg for 15 minutes at 4°C. The protein pellet was resuspended in 25 µL NP-40 buffer containing protease inhibitor. Bolt™ LDS sample buffer (#B0007; Thermo Fisher Scientific) mixed with Bolt™ Sample Reducing Agent (#B0009; Thermo Fisher Scientific) was added to the samples prior to gel electrophoresis. For analysis of intracellular dimer formation the reducing agent was omitted. Samples were heated for 5 minutes at 70°C. Supernatants from HEK293T cells transfected with ADA2 were diluted 1:10 in 2X Bolt™ LDS sample buffer (#B0007; Thermo Fisher Scientific), serum was diluted 1:200. SeeBlue™ Plus2 Pre-stained Protein Standard (#LC5925; Thermo Fisher Scientific) was used as protein molecular weight marker.
Proteins were transferred onto PVDF transfer membranes. The membranes were probed with the following primary antibodies: anti-ADA2 (clone EPR25430-131, #ab288296, 1:1000; abcam), anti-ADA2 (#HPA007888, 1:500; Sigma-Aldrich; RRID: AB_1078495), Clone OTI4C5, anti-DDK (FLAG) (clone OTI4C5, #TA50011, 1:1000; OriGene Technologies; RRID: AB_2622345), anti-LC3B (#ab51520, 1:1000; abcam; RRID: AB_881429), anti-BiP (#3183, 1:1000; Cell Signaling; RRID: AB_10695864), anti-GAPDH (clone 7B, #sc-69778, 1:500; Santa Cruz Biotechnology; RRID: AB_1124759), anti-β-actin (clone: AC-15, #A5441, 1:9,000; Sigma-Aldrich; RRID: AB_476744) at 4°C overnight or at room temperature for two hours. The membranes were washed and incubated with the respective HRP-coupled secondary antibodies for one hour at room temperature: goat anti-rabbit IgG H&L (#ab205718, 1:5000; abcam; RRID: AB_2819160), Goat Anti-Mouse IgG (H + L) (#71045, 1:5000; Sigma-Aldrich; RRID: AB_11211441) or VeriBlot Detection Reagent (#ab131366, 1:1000 in tris saline/5% skim milk ; abcam). Protein expression was visualized by enzymatic chemiluminescence using Pierce™ ECL western blotting substrate (#32106; Thermo Fisher Scientific) or SuperSignal™ West Pico PLUS Chemiluminescent Substrate (#34580; Thermo Fisher Scientific) in a ChemiDoc XRS+ Imaging System (Bio-Rad).

Glycan removal

Glycan removal was performed on whole cell lysates generated with NP-40 lysis buffer or precipitated supernatant protein reconstituted in NP-40 lysis buffer. Glycan removal was performed on 20 µg or 25 µg total protein using PNGase F (#P0704; New England Biolabs), Endo H (#P0702; New England Biolabs) or PNGase F (#A39245; Gibco) according to the manufacturer's instructions. Glycan removal with PNGase F (#P0704; New England Biolabs) was completed under denaturing conditions for 1h at 37°C or under non-denaturing conditions for 4h at 37°C as indicated.

Immunoprecipitation

Whole cell lysates were prepared from HEK293T cells transfected with wild-type ADA2 or the variants p.R169Q or HMDM from HC or DADA2 patients in NP-40 lysis buffer at a protein concentration of 1 mg/mL. Primary antibodies were added to 1000 µg lysate or 500 µg lysate, respectively, and incubated rotating at 4°C overnight. Alternatively, 1 mL supernatant was directly incubated with the primary antibodies. After overexpression, tagged ADA2 was pulled down using 1 µg anti-DDK (FLAG) clone OTI4C5 (#TA50011, OriGene Technologies). An isotype control

sample was incubated with 1 μg mouse IgG1 (#02-6100; Invitrogen) in parallel. Endogenous ADA2 was pulled down using 1 μg anti-ADA2 (clone EPR25430-131, #ab288296, abcam) with rabbit monoclonal IgG (clone EPR25A, #ab172730; abcam) used as isotype control. For immunoprecipitation, the samples were rotated with 100 μL SureBeads™ Protein G Magnetic Beads (#1614023, Bio-Rad) for 1h at room temperature. The beads were magnetized and washed four times with PBS/0.1% Tween 20. Samples for mass spectrometric analysis were washed twice with NP-40 lysis buffer and twice with PBS. For western blot, the samples were eluted from the beads in Bolt™ LDS sample buffer (#B0007; Thermo Fisher Scientific).

Protein digest

Beads from immunoprecipitation experiments were resuspended in 20 μL denaturation buffer (6 M Urea, 2 M Thiourea, 10 mM HEPES, pH 8.0), reduced for 30 min at 25°C in 12 mM dithiothreitol, followed by alkylation with 40 mM chloroacetamide for 20 min at 25 °C. Samples were first digested with 0.5 μg endopeptidase LysC (Wako, Osaka, Japan) for 4 h. After diluting the samples with 80 μL 50 mM ammonium bicarbonate (pH 8.5), 1 μg sequence grade trypsin (Promega) was added overnight at 25 °C. The peptide-containing supernatant was collected and acidified with formic acid (1% final concentration) to stop the digestion. Peptides were desalted and cleaned up using Stage Tip protocol (Rappsilber et al., 2003). After elution with 80% acetonitrile/0.1% formic acid, samples were dried using speedvac, resolved in 3% acetonitrile/0.1% formic acid and analysed by LC-MS/MS.

LC-MS/MS analyses

Peptides were separated on a reversed-phase column (20 cm fritless silica microcolumns with an inner diameter of 75 μm, packed with ReproSil-Pur C18-AQ 3 μm resin (Dr. Maisch GmbH) using a 90 min gradient with a 250 nL/min flow rate of increasing Buffer B concentration (from 2% to 60%) on a High-Performance Liquid Chromatography (HPLC) system (Thermo Fisher Scientific) and ionized using an electrospray ionization (ESI) source (Thermo Fisher Scientific) and analyzed on a Thermo Q Exactive HF-X instrument (*HEK293T*) or on an Q Exactive Plus instrument (*HMDM*). The Q Exactive HF-X instrument was run in data dependent mode selecting the top 20 most intense ions in the MS full scans, selecting ions from 350 to 2000 m/z, using 60 K resolution with a 3×10^6 ion count target and 10 ms injection time. Tandem MS was performed at a resolution of 15 K. The MS2 ion count target was set to 1×10^5 with a maximum injection time of 100 ms. Only precursors with charge state 2–6 were selected for MS2. The dynamic exclusion duration was set to 30 s with a 10-ppm tolerance around the selected precursor and its isotopes. The Q Exactive Plus instrument was run in data dependent mode selecting the top 10 most intense ions in the MS full scans, selecting ions from 350 to 2000 m/z, using 70 K resolution with a 3×10^6 ion count target and 50 ms injection time. Tandem MS was performed at a resolution of 17.5 K. The MS2 ion count target was set to 5×10^4 with a maximum injection time of 250 ms. Only precursors with charge state 2–6 were selected for MS2. The dynamic exclusion duration was set to 30 s with a 10-ppm tolerance around the selected precursor and its isotopes.

Raw data were analyzed using MaxQuant software package (v1.6.3.4) (Tyanova et al., 2016a). The internal Andromeda search engine was used to search MS2 spectra against a human UniProt database (HUMAN.2020-06), including ADA2 mutant sequence, containing forward and reverse sequences. The search included variable modifications of methionine oxidation, N-terminal acetylation and fixed modification of carbamidomethyl cysteine. The FDR was set to 1% for peptide and protein identifications. Unique and razor peptides were considered for quantification.

The LFQ (label-free quantitation) algorithm was activated. The resulting text file was filtered to exclude reverse database hits, potential contaminants, and proteins only identified by site.
The mass spectrometry data have been deposited to the ProteomeXchange Consortium via the PRIDE partner repository with the dataset identifier PXD046128.

SomaScan Assay

Serum samples (55 µL) from 12 healthy controls, 9 heterozygous ADA2 carriers and 12 DADA2 patients were sent for protein analysis by the 7,000-plex SomaScan® Assay (SomaLogic, Inc.). For several individuals, samples from multiple time points were included. The cohort details are presented in **Table S2**. The assay readout was provided in relative fluorescent units (RFU) for all measured aptamers for each serum sample.

ADA2 enzyme activity

Adenosine deaminase 2 enzyme activity was determined in whole cell lysates from HEK293T cells overexpressing ADA2 or HMDM with and without glycan removal as well as in supernatants from transfected HEK293T cells and human serum. Deaminase activity was measured in a colorimetric assay adapted from Giusti and Galanti (Illingworth, 1985). Erythro-9-(2-hydroxy-3-nonyl) adenine (EHNA) (#E114; Sigma-Aldrich) was used to inhibit ADA1 activity. Triplicate measurements were performed for all samples. Enzymatic activity of pathogenic ADA2 variants overexpressed HEK293T cells was normalized to the activity of wild-type ADA2.

qPCR

5-10x10^5 cells were lysed in TRIzol™ Reagent (#15596018; Thermo Fisher Scientific) for 3 minutes at room temperature and homogenized before storage at -80°C. To measure the ER stress response, HEK293T cells were seeded at 5x104 cells/ml in a 24-well plate 24h prior to transfection. TRIzol™ samples were prepared 48h after transfection. RNA was extracted using the PureLink™ RNA Mini Kit (#12183018A; Thermo Fisher Scientific) according to the manufacturer's instruction. cDNA was generated from 20 ng RNA using the SuperScript™ VILO™ cDNA Synthesis Kit (#11754050; Thermo Fisher Scientific). Quantitative polymerase chain reaction (qPCR) analysis was performed with SsoAdvanced™ Universal SYBR® Green Supermix (#1725271; Bio-Rad Laboratories) and the following primers:
ADA2(929-1038)_F_GGCTCCGAATCAAGTTCCCC;
ADA2(929-1038)_R_TAAGGCAGCTTAACGCCATCC;
ADA2(1138-1257)_F_ACCAGAATCGGCCATGGA;
ADA2(1138-1257)_R_CTACAGGGTGGTTCCTCAAGTCA;
HSPA5_F_CAAGCAACCAAAGACGCTGGA; HSPA5_R_GCCACCCAGGTCAAACACCA; DDIT3_F_AGAGGAAGAATCAAAAATCT; DDIT3_R_AGCTCTGACTGGAATCTGGA; GAPDH_F_GTCTCCTCTGACTTCAACAGCG;
GAPDH_R_ACCACCCTGTTGCTGTAGCCAA. For all conditions, three technical replicates were measured. The experiment was run on a QuantStudio™ 3 Real-Time PCR System (Thermo Fisher Scientific) and analyzed using the QuantStudio™ Design & Analysis Software v1.5.2. The relative abundance of *ADA2* was normalized to the expression level of *GAPDH*. and different conditions were compared using the $2^{-\Delta\Delta Ct}$ method (Livak and Schmittgen, 2001).

Statistical analysis

For the SomaScan assay, raw counts expressed in relative fluorescent units (RFU) were normalized across samples using a cyclic loess algorithm implemented by the package limma (Ritchie et al., 2015). Two outlier samples identified with principal component analysis were removed before downstream analysis. Differentially expressed genes were identified using a linear model based on subject condition (HC, Carrier, DADA2), subject age, and number of freeze-thaw-cycles of the sample. Pseudoreplicates coming from subjects with multiple samples were handled using blocking. Statistics were moderated using the empirical Bayes method of the package limma (Ritchie et al., 2015).

Statistical analysis of the mass spectrometry data was performed using Perseus software (v1.6.2.1) (Tyanova et al., 2016b). Log2 transformed LFQ intensity values were filtered for minimum of 3 valid values in at least one experimental group and missing values were imputed with random low intensity values taken from a normal distribution. Differences in protein abundance between groups were calculated using two-sample Student's t-test using an FDR-based significance cut-off of 5% (*HEK293T*) or 10% (*HMDM*) in order to define enriched proteins.

Online supplemental material

The online supplementary information provides additional data on the expression and glycosylation of ADA2 in immune cell lines as well as healthy control and DADA2 HMDM (**Figure S1**). **Figure S2** highlights the superior binding capacity of the anti-ADA2 antibody clone EPR25430-131 (#ab288296; abcam) for LMW-ADA2. **Figure S3** provides supplementary data describing the interactome and ER stress experiments.

Data availability

The mass spectrometry data have been deposited to the ProteomeXchange Consortium via the PRIDE partner repository with the dataset identifier PXD046128. Further information are available upon request.

Acknowledgments

We thank Prof. Jaak Jaeken, Prof. Daisy Rymen and Dr. Eva Morava-Kozicz for kindly sharing their expertise and insight on protein glycosylation. We thank Lotte Bral for her assistance in the production of the knock-out cell lines. Above all, we would like to express our gratitude to our patients and their parents for their willingness to participate in our study and to their treating physicians and nurses for their efforts in the collection of research samples. The graphical abstract was created with BioRender.com.

Author contributions

LE, LM and IM were responsible for the study conception and design. Material preparation and data collection was performed by LE, AH, MW, BP, SD, MD, MK and LM. LE, AH, MB, MK and LM performed the data analysis. MJ and DD assisted in the generation of ADA2 knock-out cell lines. The proteomics analyses were performed in collaboration with MK, PM and TM. PA supported the design of the ER stress experiments. LE, SD, GB, LDS, RS, SV, DC and IM collected clinical data and biological materials from patients. The first draft of the manuscript was

written by LE. All authors reviewed the manuscript and approved its submission. IM is responsible for the supervision of the study.

Disclosures

This project has received funding from the European Research Council (ERC) under the European Union's Horizon 2020 research and innovation program (GA No. 948959) (MORE2ADA2). IM is a Senior Clinical Investigator at the Research Foundation–Flanders, and is supported by a KU Leuven C1 Grant [grant number C16/18/007]; by the Research Foundation-Flanders (FWO) [grant number G0B5120N]; and by the Jeffrey Modell Foundation. This work was supported by ERN-RITA. LE is supported by a PhD Fellowship from the Research Foundation – Flanders (FWO) (grant 11E0123N). SD is supported by a PhD Fellowship from the Research Foundation – Flanders (FWO) (grant 11F4421N). RS is a FWO senior clinical investigator fellow (1805523N). PA is supported by grants from the Flemish Research Foundation (FWO-Vlaanderen G0A3320N), the KU Leuven C14/21/095 InterAction consortium, the EOS MetaNiche consortium N° 40007532, the iBOF/21/053 ATLANTIS network and by the EOS DECODE consortium N° 30837538.

References

Bowers, S.M., M. Sundqvist, P. Dancey, D.A. Cabral, and K.L. Brown. 2022. Pathogenic variant c.1052T>A (p.Leu351Gln) in adenosine deaminase 2 impairs secretion and elevates type I IFN responsive gene expression. *Front. Immunol.* 13.

Boya, P., R.-A. González-Polo, N. Casares, J.-L. Perfettini, P. Dessen, N. Larochette, D. Métivier, D. Meley, S. Souquere, T. Yoshimori, G. Pierron, P. Codogno, and G. Kroemer. 2005. Inhibition of Macroautophagy Triggers Apoptosis. *Mol. Cell. Biol.* 25:1025–1040. doi:10.1128/MCB.25.3.1025-1040.2005.

Carmona-Rivera, C., S.S. Khaznadar, K.W. Shwin, J.A. Irizarry-Caro, L.J. O'Neil, Y. Liu, K.A. Jacobson, A.K. Ombrello, D.L. Stone, W.L. Tsai, D.L. Kastner, I. Aksentijevich, M.J. Kaplan, and P.C. Grayson. 2019. Deficiency of adenosine deaminase 2 triggers adenosine-mediated NETosis and TNF production in patients with DADA2. *Blood.* 134:395–406. doi:10.1182/blood.2018892752.

Chen, L., A. Mamutova, A. Kozlova, E. Latysheva, F. Evgeny, T. Latysheva, K. Savostyanov, A. Pushkov, I. Zhanin, E. Raykina, M. Kurnikova, I. Mersiyanova, C.D. Platt, H. Jee, K. Brodeur, Y. Du, M. Liu, A. Weiss, G.S. Schulert, J. Rodriguez-Smith, M.S. Hershfield, I. Aksentijevich, Q. Zhou, P.A. Nigrovic, A. Shcherbina, E. Alexeeva, and P.Y. Lee. 2023. Comparison of disease phenotypes and mechanistic insight on causal variants in patients with DADA2. *J. Allergy Clin. Immunol.* doi:10.1016/j.jaci.2023.04.014.

Daniels, M.A., K.A. Hogquist, and S.C. Jameson. 2002. Sweet "n" sour: the impact of differential glycosylation on T cell responses. *Nat. Immunol.* 3:903–910. doi:10.1038/ni1002-903.

Davidson, S., C.-H. Yu, A. Steiner, F. Ebstein, P.J. Baker, V. Jarur-Chamy, K. Hrovat Schaale, P. Laohamonthonkul, K. Kong, D.J. Calleja, C.R. Harapas, K.R. Balka, J. Mitchell, J.T. Jackson, N.D. Geoghegan, F. Moghaddas, K.L. Rogers, K.D. Mayer-Barber, A.A. De Jesus, D. De Nardo, B.T. Kile, A.J. Sadler, M.C. Poli, E. Krüger, R. Goldbach Mansky, and S.L. Masters. 2022. Protein kinase R is an innate immune sensor of proteotoxic stress via accumulation of cytoplasmic IL-24. *Sci. Immunol.* 7:eabi6763. doi:10.1126/sciimmunol.abi6763.

Deuitch, N.T., D. Yang, P.Y. Lee, X. Yu, N.S. Moura, O. Schnappauf, A.K. Ombrello, D. Stone, H.S. Kuehn, S.D. Rosenzweig, P. Hoffmann, C. Cudrici, D.M. Levy, E. Kessler, J.B. Soep, A.D. Hay, A. Dalrymple, Y. Zhang, L. Sun, Q. Zhang, X. Tang, Y. Wu, K. Rao, H. Li, H. Luo, Y. Zhang, J.M. Burnham, M. Boehm, K. Barron, D.L. Kastner, I. Aksentijevich, and Q. Zhou. 2022. TNF inhibition in vasculitis management in adenosine deaminase 2 deficiency (DADA2). *J. Allergy Clin. Immunol.* 149:1812-1816.e6. doi:10.1016/j.jaci.2021.10.030.

Dhanwani, R., M. Takahashi, I.T. Mathews, C. Lenzi, A. Romanov, J.D. Watrous, B. Pieters, C.C. Hedrick, C.A. Benedict, J. Linden, R. Nilsson, M. Jain, and S. Sharma. 2020. Cellular sensing of extracellular purine nucleosides triggers an innate IFN-β response. *Sci. Adv.* 6:eaba3688. doi:10.1126/sciadv.aba3688.

Doench, J.G., N. Fusi, M. Sullender, M. Hegde, E.W. Vaimberg, K.F. Donovan, I. Smith, Z. Tothova, C. Wilen, R. Orchard, H.W. Virgin, J. Listgarten, and D.E. Root. 2016. Optimized sgRNA design to maximize activity and minimize off-target effects of CRISPR-Cas9. *Nat. Biotechnol.* 34:184–191. doi:10.1038/nbt.3437.

Fiedorczuk, K., and J. Chen. 2022. Mechanism of CFTR correction by type I folding correctors. *Cell.* 185:158-168.e11. doi:10.1016/j.cell.2021.12.009.

Fujiwara, T., K. Oda, S. Yokota, A. Takatsuki, and Y. Ikehara. 1988. Brefeldin A causes disassembly of the Golgi complex and accumulation of secretory proteins in the endoplasmic reticulum. *J. Biol. Chem.* 263:18545–18552. doi:10.1016/S0021-9258(19)81393-5.

Greiner-Tollersrud, O.K., V. Boehler, E. Bartok, M. Krausz, A. Polyzou, J. Schepp, M. Seidl, J.O. Olsen, C.R. Smulski, S. Raieli, K. Hübscher, E. Trompouki, R. Link, H. Ebersbach, H. Srinivas, M. Marchant, D. Staab, D. Guerini, S. Baasch, P. Henneke, G. Kochs, G. Hartmann, R. Geiger, B. Grimbacher, M. Warncke, and M. Proietti. 2020. ADA2 is a lysosomal DNase regulating the type-I interferon response.

Hashem, H., A.R. Kumar, I. Müller, F. Babor, R. Bredius, J. Dalal, A.P. Hsu, S.M. Holland, D.D. Hickstein, S. Jolles, R. Krance, G. Sasa, M. Taskinen, M. Koskenvuo, J. Saarela, J. van Montfrans, K. Wilson, B. Bosch, L. Moens, M. Hershfield, and I. Meyts. 2017. Hematopoietic stem cell transplantation rescues the hematological, immunological, and vascular phenotype in DADA2. *Blood.* 130:2682–2688. doi:10.1182/blood-2017-07-798660.

Illingworth, J. 1985. Methods of enzymatic analysis: Third edition: Editor-in-Chief: Hans Ulrich Bergmeyer. Verlag Chemie, 1983 (vols I–III), 1984 (vols IV & V) DM258 each volume or DM2240 vols I–X inclusive. *Biochem. Educ.* 13:38–38. doi:10.1016/0307-4412(85)90136-0.

Infevers: an online database for autoinflammatory mutations. Copyright. Available at https://infevers.umai-montpellier.fr/ Accessed 14/08/2023.

Ito, M., Y. Maejima, K. Nishimura, Y. Nakae, A. Ono, and S. Iwaki-Egawa. 2022. A role for N-glycosylation in active adenosine deaminase 2 production. *Biochim. Biophys. Acta BBA - Gen. Subj.* 1866:130237. doi:10.1016/j.bbagen.2022.130237.

Jee, H., Z. Huang, S. Baxter, Y. Huang, M.L. Taylor, L.A. Henderson, S. Rosenzweig, A. Sharma, E.P. Chambers, M.S. Hershfield, Q. Zhou, F. Dedeoglu, I. Aksentijevich, P.A. Nigrovic, A. O'Donnell-Luria, and P.Y. Lee. 2021. Comprehensive analysis of ADA2 genetic variants and estimation of carrier frequency driven by a function-based approach. *J. Allergy Clin. Immunol.* doi:10.1016/j.jaci.2021.04.034.

Karczewski, K.J., L.C. Francioli, G. Tiao, B.B. Cummings, J. Alföldi, Q. Wang, R.L. Collins, K.M. Laricchia, A. Ganna, D.P. Birnbaum, L.D. Gauthier, H. Brand, M. Solomonson, N.A. Watts, D. Rhodes, M. Singer-Berk, E.M. England, E.G. Seaby, J.A. Kosmicki, R.K. Walters, K. Tashman, Y. Farjoun, E. Banks, T. Poterba, A. Wang, C. Seed, N. Whiffin, J.X. Chong, K.E. Samocha, E. Pierce-Hoffman, Z. Zappala, A.H. O'Donnell-Luria, E.V. Minikel, B. Weisburd, M. Lek, J.S. Ware, C. Vittal, I.M. Armean, L. Bergelson, K. Cibulskis, K.M. Connolly, M. Covarrubias, S. Donnelly, S. Ferriera, S. Gabriel, J. Gentry, N. Gupta, T.

Jeandet, D. Kaplan, C. Llanwarne, R. Munshi, S. Novod, N. Petrillo, D. Roazen, V. Ruano-Rubio, A. Saltzman, M. Schleicher, J. Soto, K. Tibbetts, C. Tolonen, G. Wade, M.E. Talkowski, B.M. Neale, M.J. Daly, and D.G. MacArthur. 2020. The mutational constraint spectrum quantified from variation in 141,456 humans. *Nature*. 581:434–443. doi:10.1038/s41586-020-2308-7.

Kim, M.-S., and D. Leahy. 2013. Chapter Nineteen - Enzymatic Deglycosylation of Glycoproteins. *In* Methods in Enzymology. J. Lorsch, editor. Academic Press. 259–263.

Kirchner, P., M. Bourdenx, J. Madrigal-Matute, S. Tiano, A. Diaz, B.A. Bartholdy, B. Will, and A.M. Cuervo. 2019. Proteome-wide analysis of chaperone-mediated autophagy targeting motifs. *PLOS Biol.* 17:e3000301. doi:10.1371/journal.pbio.3000301.

Lee, P.Y., Y. Huang, Q. Zhou, O. Schnappauf, M.S. Hershfield, Y. Li, N.J. Ganson, N. Sampaio Moura, O.M. Delmonte, S.S. Stone, M.J. Rivkin, S.-Y. Pai, T. Lyons, R.P. Sundel, V.W. Hsu, L.D. Notarangelo, I. Aksentijevich, and P.A. Nigrovic. 2018. Disrupted N-linked glycosylation as a disease mechanism in deficiency of ADA2. *J. Allergy Clin. Immunol.* 142:1363-1365.e8. doi:10.1016/j.jaci.2018.05.038.

Lee, P.Y., E.S. Kellner, Y. Huang, E. Furutani, Z. Huang, W. Bainter, M.F. Alosaimi, K. Stafstrom, C.D. Platt, T. Stauber, S. Raz, I. Tirosh, A. Weiss, M.B. Jordan, C. Krupski, D. Eleftheriou, P. Brogan, A. Sobh, Z. Baz, G. Lefranc, C. Irani, S.S. Kilic, R. El-Owaidy, M.R. Lokeshwar, P. Pimpale, R. Khubchandani, E.P. Chambers, J. Chou, R.S. Geha, P.A. Nigrovic, and Q. Zhou. 2020. Genotype and functional correlates of disease phenotype in deficiency of adenosine deaminase 2 (DADA2). *J. Allergy Clin. Immunol.* 145:1664-1672.e10. doi:10.1016/j.jaci.2019.12.908.

Livak, K.J., and T.D. Schmittgen. 2001. Analysis of relative gene expression data using real-time quantitative PCR and the 2(-Delta Delta C(T)) Method. *Methods San Diego Calif.* 25:402–408. doi:10.1006/meth.2001.1262.

Meyts, I., and I. Aksentijevich. 2018. Deficiency of Adenosine Deaminase 2 (DADA2): Updates on the Phenotype, Genetics, Pathogenesis, and Treatment. *J. Clin. Immunol.* 38:569–578. doi:10.1007/s10875-018-0525-8.

Mollenhauer, H.H., D. James Morré, and L.D. Rowe. 1990. Alteration of intracellular traffic by monensin; mechanism, specificity and relationship to toxicity. *Biochim. Biophys. Acta BBA - Rev. Biomembr.* 1031:225–246. doi:10.1016/0304-4157(90)90008-Z.

Navon Elkan, P., S.B. Pierce, R. Segel, T. Walsh, J. Barash, S. Padeh, A. Zlotogorski, Y. Berkun, J.J. Press, M. Mukamel, I. Voth, P.J. Hashkes, L. Harel, V. Hoffer, E. Ling, F. Yalcinkaya, O. Kasapcopur, M.K. Lee, R.E. Klevit, P. Renbaum, A. Weinberg-Shukron, E.F. Sener, B. Schormair, S. Zeligson, D. Marek-Yagel, T.M. Strom, M. Shohat, A. Singer, A. Rubinow, E. Pras, J. Winkelmann, M. Tekin, Y. Anikster, M.-C. King, and E. Levy-Lahad. 2014. Mutant adenosine deaminase 2 in a polyarteritis nodosa vasculopathy. *N. Engl. J. Med.* 370:921–931. doi:10.1056/NEJMoa1307362.

Pakos-Zebrucka, K., I. Koryga, K. Mnich, M. Ljujic, A. Samali, and A.M. Gorman. 2016. The integrated stress response. *EMBO Rep.* 17:1374–1395. doi:10.15252/embr.201642195.

Pankow, S., C. Bamberger, D. Calzolari, S. Martínez-Bartolomé, M. Lavallée-Adam, W.E. Balch, and J.R. Yates. 2015. ΔF508 CFTR interactome remodelling promotes rescue of cystic fibrosis. *Nature*. 528:510–516. doi:10.1038/nature15729.

Rappsilber, J., Y. Ishihama, and M. Mann. 2003. Stop and go extraction tips for matrix-assisted laser desorption/ionization, nanoelectrospray, and LC/MS sample pretreatment in proteomics. *Anal. Chem.* 75:663–670. doi:10.1021/ac026117i.

Ritchie, M.E., B. Phipson, D. Wu, Y. Hu, C.W. Law, W. Shi, and G.K. Smyth. 2015. limma powers differential expression analyses for RNA-sequencing and microarray studies. *Nucleic Acids Res.* 43:e47. doi:10.1093/nar/gkv007.

Rubinsztein, D.C. 2006. The roles of intracellular protein-degradation pathways in neurodegeneration. *Nature*. 443:780–786. doi:10.1038/nature05291.

Tarrant, T.K., S.J. Kelly, and M.S. Hershfield. 2022. Elucidating the pathogenesis of adenosine deaminase 2 deficiency: current status and unmet needs. *Expert Opin. Orphan Drugs*. 0:null. doi:10.1080/21678707.2021.2050367.

Tyanova, S., T. Temu, and J. Cox. 2016a. The MaxQuant computational platform for mass spectrometry-based shotgun proteomics. *Nat Protoc.* 11:2301–2319. doi:10.1038/nprot.2016.136.

Tyanova, S., T. Temu, P. Sinitcyn, A. Carlson, M.Y. Hein, T. Geiger, M. Mann, and J. Cox. 2016b. The Perseus computational platform for comprehensive analysis of (prote)omics data. *Nat. Methods*. 13:731–740. doi:10.1038/nmeth.3901.

Watanabe, N., S. Gao, Z. Wu, S. Batchu, S. Kajigaya, C. Diamond, L. Alemu, D.Q. Raffo, P. Hoffmann, D. Stone, A.K. Ombrello, and N.S. Young. 2021. Analysis of deficiency of adenosine deaminase 2 pathogenesis based on single-cell RNA sequencing of monocytes. *J. Leukoc. Biol.* 110:409–424. doi:10.1002/JLB.3HI0220-119RR.

Zavialov, A.V., X. Yu, D. Spillmann, G. Lauvau, and A.V. Zavialov. 2010. Structural basis for the growth factor activity of human adenosine deaminase ADA2. *J. Biol. Chem.* 285:12367–12377. doi:10.1074/jbc.M109.083527.

Zhou, Q., D. Yang, A.K. Ombrello, A.V. Zavialov, C. Toro, A.V. Zavialov, D.L. Stone, J.J. Chae, S.D. Rosenzweig, K. Bishop, K.S. Barron, H.S. Kuehn, P. Hoffmann, A. Negro, W.L. Tsai, E.W. Cowen, W. Pei, J.D. Milner, C. Silvin, T. Heller, D.T. Chin, N.J. Patronas, J.S. Barber, C.-C.R. Lee, G.M. Wood, A. Ling, S.J. Kelly, D.E. Kleiner, J.C. Mullikin, N.J. Ganson, H.H. Kong, S. Hambleton, F. Candotti, M.M. Quezado, K.R. Calvo, H. Alao, B.K. Barham, A. Jones, J.F. Meschia, B.B. Worrall, S.E. Kasner, S.S. Rich, R. Goldbach-Mansky, M. Abinun, E. Chalom, A.C. Gotte, M. Punaro, V. Pascual, J.W. Verbsky, T.R. Torgerson, N.G. Singer, T.R. Gershon, S. Ozen, O. Karadag, T.A. Fleisher, E.F. Remmers, S.M. Burgess, S.L. Moir, M. Gadina, R. Sood, M.S. Hershfield, M. Boehm, D.L. Kastner, and I. Aksentijevich. 2014. Early-onset stroke and vasculopathy associated with mutations in ADA2. *N. Engl. J. Med.* 370:911–920. doi:10.1056/NEJMoa1307361.

Abbreviations

ADA2	Adenosine deaminase 2
DADA2	Deficiency of adenosine deaminase 2
Endo H	Endoglycosidase H
HC	Healthy control
HMDM	Human monocyte-derived macrophages
PNGase F	Peptide-N-Glycosidase F
TNFi	TNF inhibitors
WT	Wild type

Figure legends

Figure 1: Expression pattern of pathogenic ADA2 variants. (A) Overview of the location of all pathogenic variants of ADA2 included in this study across the *ADA2* gene and encoded protein domains. Shaded variants are present in our cohort of DADA2 patients. Stars indicate N-glycosylation sites. (B) mRNA and intracellular protein expression of ADA2 in CD14+ monocytes from healthy controls (HC) and DADA2 patients (P) by qPCR and western blot of whole cell lysates, respectively. *ADA2* mRNA expression was normalized to *GAPDH* and is depicted relative to the mean of HC samples. (C) ADA2 protein expression in whole cell lysates and supernatant (SN) of CD14+ monocytes and GM-CSF differentiated human monocyte-derived macrophages (HMDM) from healthy controls (HC), carriers (CR) and DADA2 patients (P) was determined by western blot. (D) ADA2 protein expression in supernatants (SN) from healthy control human monocyte-derived macrophages (HMDM) and serum samples from healthy controls (HC) and DADA2 patients (P) by western blot using VeriBlot for detection. (E) ADA2 protein expression in whole cell lysates of HEK293T cells after transfection with wild-type (WT) ADA2 and different pathogenic variants (left) and comparing whole cell lysates (WCE) and supernatant (SN) by western blot. The anti-ADA2 antibody clone EPR25430-131 (#ab288296; abcam) was used for detection in all depicted western blots. Triangles indicate HMW-ADA2 (red) and LMW-ADA2 (green). Legend: CD, catalytic domain; DD, dimerization domain; EV, empty vector; PRB D, putative receptor binding domain.

Figure 2: N-glycosylation pattern of ADA2. (A) Western blot of wild-type (WT) ADA2 and the pathogenic variants p.R169Q and p.T129P transfected into HEK293T cells after incubation with or without 2.5 μg/mL tunicamycin (TM) for 24h. Glycan removal was performed by incubation with PNGase F for 1 hour at 37°C under denaturing conditions. (B) ADA2 protein expression by western blot in whole cell lysates (WCE) and supernatants (SN) of human monocyte-derived macrophages (HMDM), U-937 cells and THP-1 cells. Glycan removal was performed by incubation with PNGase F for 1 hour at 37°C under denaturing conditions. (C) ADA2 protein expression in whole cell lysates and supernatants from GM-CSF-differentiated HMDM of healthy control HC8 and DADA2 patient P8 left untreated or treated with 5 μg/mL tunicamycin or 1 μg/mL brefeldin A for 24h. Glycan removal was performed by incubation with PNGase F for 1 hour at 37°C under denaturing conditions. (D) ADA2 protein expression in whole cell lysates and supernatants from U-937 and THP-1 cells left untreated or treated with 2.5 μg/mL tunicamycin or 1 μg/mL brefeldin A for 24h. Glycan removal was performed by incubation with PNGase F for 1 hour at 37°C under denaturing conditions. (E) GM-CSF-differentiated healthy control HMDM were treated with or without 5 μg/mL tunicamycin for 24h. Glycan removal was performed by incubation with PNGase F at 37°C under denaturing (1h) and non-denaturing (4h) conditions. ADA2 enzyme activity was determined in whole cell lysates handled under non-denaturing conditions. (F) HEK293T cells transfected with wild-type (WT) ADA2 or pathogenic ADA2 variants were treated with or without 2.5 μg/mL tunicamycin for 24h. Glycan removal was performed by incubation with PNGase F at 37°C under denaturing (1h) and non-denaturing (4h) conditions. ADA2 enzyme activity was determined in whole cell lysates handled under non-denaturing conditions. (G) ADA2 protein expression by western blot after glycan removal in CD14+ monocytes or GM-CSF-differentiated HMDM from healthy controls (HC) and DADA2 patient P4 by incubation with PNGase F or Endo H for 1 hour at 37°C under denaturing conditions. (H) ADA2 protein expression by western blot in GM-CSF-differentiated HMDM from healthy control HC12 and DADA2 patient P4 after incubation with 100 μg/mL castanospermine

(CAS) for 24h. (I) *Left:* ADA2 protein expression by western blot in monocyte and HMDM whole cell lysates as well as HMDM supernatants from healthy controls (HC), DADA2 heterozygous carriers (CR), DADA2 patient P4 and a patient with *PMM2*-congenital disorder of glycosylation (CDG). *Right:* ADA2 enzyme activity was determined in the serum of pediatric and adult healthy controls, DADA2 heterozygous carriers, DADA2 patients and the *PMM2*-CDG patient. In figures A-F and G (left) ADA2 was detected using anti-ADA2 (#HPA007888, Sigma-Aldrich; in figures G (right) and H+I anti-ADA2 antibody clone EPR25430-131 (#ab288296; abcam) was used. Triangles indicate HMW-ADA2 (red), LMW-ADA2 (green) and glycan-free ADA2 (dark blue). Legend: CDG, congenital disorder of glycosylation; EV, empty vector; NT, non-transfected.

Figure 3: ER stress in DADA2. (A) Interactome analysis of wild-type (WT) ADA2 and the pathogenic variant p.R169Q overexpressed in HEK293T cells treated with or without 2.5 μg/mL tunicamycin (TM) for 24h was performed by immunoprecipitation followed by mass spectrometry. Heatmap shows z-score of protein abundance. Binders significantly pulled down compared to isotype control with a false discovery rate of 5% are highlighted by colored circles. Localization of the interacting proteins to the ER/Golgi (blue) or lysosome (green) is indicated by color. (B) ER stress response in HEK293T cells transfected with wild-type (WT) ADA2 and different pathogenic variants. Protein expression of BiP (left) and mRNA expression of *HSPA5* and *DDIT3* (right) were determined 48h after transfection. mRNA expression was normalized to *GAPDH* and is depicted as $2^{-\Delta\Delta Ct}$ relative to non-transfected control samples. Results from 6 independent experiments are shown. (C) ER stress response was evaluated by protein expression of BiP in whole cell lysates of CD14+ monocytes at baseline or after 24h incubation with or without 1 μg/mL tunicamycin (TM). BiP expression was normalized to β-actin. ADA2 was detected by anti-ADA2 antibody clone EPR25430-131 (#ab288296; abcam). Legend: EV, empty vector; FC, fold change; NT, non-transfected.

Figure 4: Trafficking and glycosylation of ADA2. (A) HEK293T cells were transfected with wild-type (WT) ADA2 or the pathogenic variant p.R169Q and treated with 2.5 μg/mL tunicamycin (TM) over 48h. Whole cell lysates were generated at the indicated time points and immunoblotted for ADA2 expression. (B) HEK293T cells were transfected with wild-type (WT) ADA2 or different pathogenic variants and treated with 2.5 μg/mL tunicamycin (TM) over 24h. Whole cell lysates were generated at the indicated time points and immunoblotted for ADA2 expression. (C) HEK293T cells were transfected with wild-type (WT) ADA2 or different pathogenic variants and treated with 500 μg/mL cycloheximide (CHX) over 24h. Whole cell lysates were generated at the indicated time points and immunoblotted for ADA2 expression. (D) ADA2 protein levels were determined in supernatants of M-CSF-differentiated human monocyte-derived macrophages (HMDM) from healthy controls (HC) or DADA2 patients (P) or HEK293T cells transfected with wild-type (WT) ADA2 or different pathogenic ADA2 variants. The patients' genotypes are indicated above. ADA2 enzyme activity was determined in the supernatant. Western blot of serum samples from healthy controls (HC), heterozygous DADA2 carriers (CR) and DADA2 patients (P) detected by anti-ADA2 antibody clone EPR25430-131 (#ab288296; abcam) and VeriBlot. (E) HEK293T cells were transfected with wild-type (WT) ADA2 or the pathogenic variant p.R169Q and treated with 500 μg/mL cycloheximide (CHX) over 24h. Supernatant was collected at the indicated time points and ADA2 levels were determined by western blot. (F) HEK293T cells were transfected with wild-type (WT) ADA2 or different pathogenic variants and treated with 500 μg/mL cycloheximide (CHX) ± 1 μg/mL brefeldin A (BFA) over 24h. Whole cell lysates were generated at the indicated time points and immunoblotted for ADA2 expression. Triangles indicate HMW-ADA2 (red), LMW-ADA2 (green) and glycan-free ADA2 (dark blue). In figures A+B ADA2 was detected using anti-

ADA2 (#HPA007888, Sigma-Aldrich); in figures C-F anti-ADA2 antibody clone EPR25430-131 (#ab288296; abcam) was used. Legend: EV, empty vector; MWM, molecular weight marker.

Figure 5: Intracellular dimer formation and secretion of mutant ADA2. (A) ADA2 protein expression and formation of intracellular dimers in HEK293T cells transfected with wild-type (WT) ADA2 and different pathogenic ADA2 variants. The blot is equivalent to the one shown in Figure 1E. (B) ADA2 protein expression and formation of intracellular dimers in HEK293T cells transfected with wild-type (WT) ADA2 and different pathogenic ADA2 variants with or without treatment with 2.5 μg/mL tunicamycin (TM) or 1 μg/mL brefeldin A (BFA) for 24h. ADA2 was detected using anti-ADA2 (#HPA007888, Sigma-Aldrich. (C) ADA2 protein expression and intracellular dimer formation in GM-CSF (left) or M-CSF (right) differentiated human monocyte-derived macrophages from healthy controls (HC) and DADA2 patients (P) with or without treatment with 5 μg/mL tunicamycin (TM) or 1 μg/mL brefeldin A (BFA) for 24h. (D) HEK293T cells were transfected with a total of 100 ng plasmid DNA of WT ADA2 or the pathogenic variant p.R169Q at the indicated ratios. ADA2 protein levels were determined in supernatant (upper blot) or whole cell lysate (middle blot) using anti-ADA2 antibody clone EPR25430-131 (#ab288296; abcam) and anti-DDK (FLAG) clone OTI4C5 (#TA50011, OriGene Technologies), respectively. (E) ADA2 serum protein levels in serum of healthy controls, carriers and DADA2 patient were determined by SomaScan assay. Measurements are depicted as relative fluorescent units (RFU) that are directly proportional to the amount of target protein in the sample. For several patients, multiple samples from different time points were included. (F) ADA2 protein expression in whole cell lysates of CD14+ monocytes from healthy control (HC) and DADA2 heterozygous carriers (CR) by western blot, normalized to β-actin. In figures A, C and F ADA2 was detected using anti-ADA2 antibody clone EPR25430-131 (#ab288296; abcam). Legend: EV, empty vector.

Figure 6: Expression of mutant ADA2 upon inhibition of the secretory pathway. (A) HEK293T cells were transfected with wild-type (WT) ADA2 or the pathogenic variant p.R169Q and treated with 500 μg/mL cycloheximide (CHX) ± 2 μg/mL monensin for 24h. Whole cell lysates were generated at the indicated time points and immunoblotted for ADA2 expression. (B) ADA2 protein expression in GM-CSF-differentiated human monocyte-derived macrophages from healthy controls (HC) or DADA2 patient P4 left untreated or treated with 1 μg/mL brefeldin A (BFA) or 2 μg/mL monensin (MN). (C) HEK293T cells were transfected with wild-type (WT) ADA2 or the pathogenic variant p.R169Q and treated with the following reagents for 24h as indicated: 50 μM chloroquine (CQ), 2 μg/mL monensin (MN), 1 μg/mL brefeldin A (BFA), 200 nM delanzomib (DZM). Whole cell lysates were immunoblotted for ADA2 expression. (D) HMDM from DADA2 patient P6 were generated by differentiation with 20 ng/mL GM-CSF for 10 days followed by 24-hour incubation with the following reagents: 1 μg/mL brefeldin A (BFA), 50 μM chloroquine (CQ), 200 nM delanzomib (DZM), 2 μg/mL monensin (MN). Whole cell lysates were immunoblotted for ADA2 expression. The western blot is representative of n=2 independent experiments. Triangles indicate HMW-ADA2 (red) and LMW-ADA2 (green). ADA2 was detected using anti-ADA2 antibody clone EPR25430-131 (#ab288296; abcam) in all depicted blots. Legend: MWM, molecular weight marker.

Figures

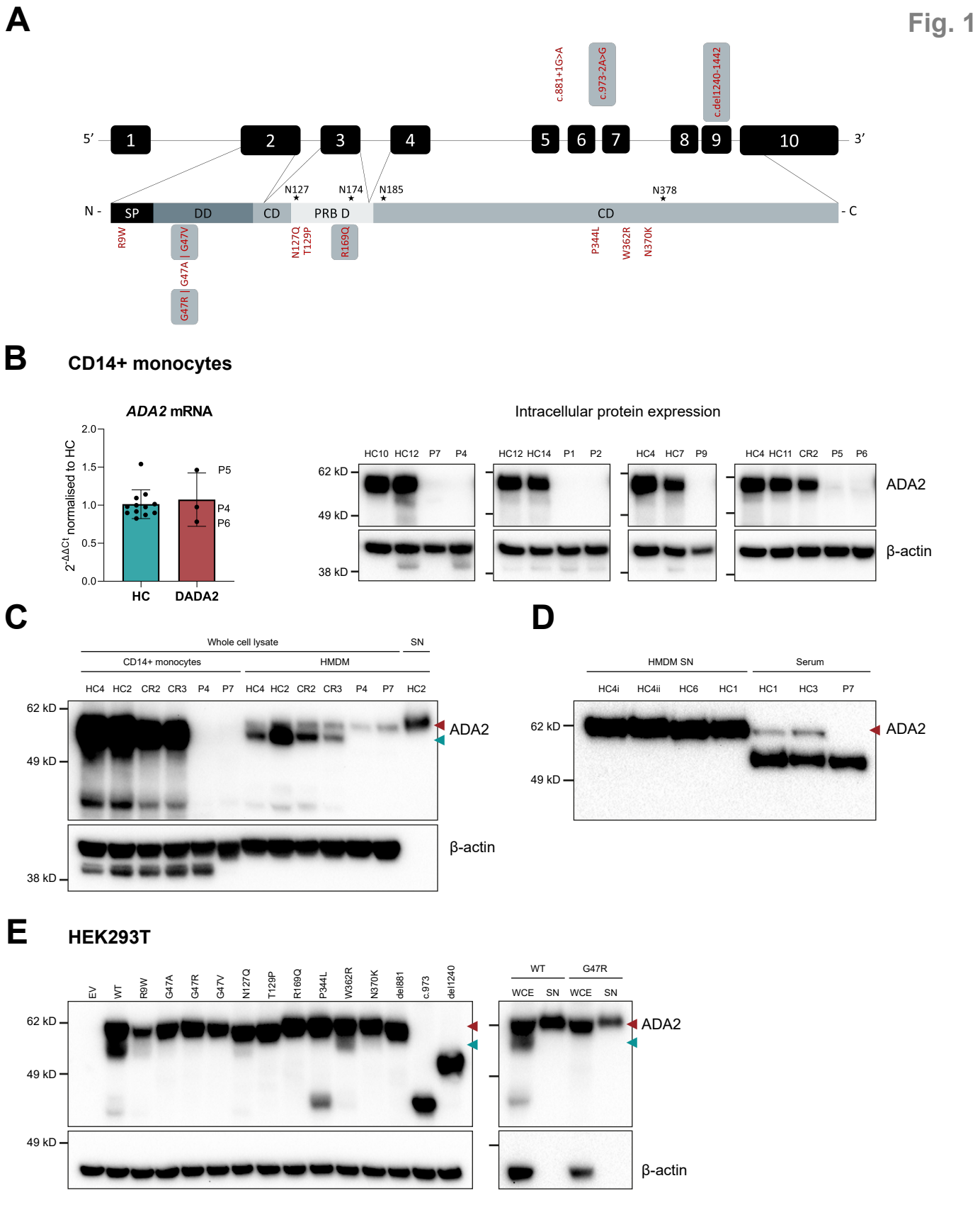
A
c.881+1G>A
c.973-2A>G
c.del1240-1442
5'
1
2
3
4
5
6
7
8
9
10
3'
N127
N174
N185
N378
N -
SP
DD
CD
PRB D
CD
- C
R9W
G47V
G47A
G47R
N127Q
T129P
R169Q
P344L
W362R
N370K
B
CD14+ monocytes
ADA2 mRNA
2-ΔΔCt normalised to HC
2.0
1.5
1.0
0.5
0.0
P5
P4
P6
HC
DADA2
Intracellular protein expression
HC10 HC12 P7 P4
HC12 HC14 P1 P2
HC4 HC7 P9
HC4 HC11 CR2 P5 P6
62 kD
49 kD
38 kD
ADA2
β-actin
C
Whole cell lysate
SN
CD14+ monocytes
HMDM
HC4 HC2 CR2 CR3 P4 P7 HC4 HC2 CR2 CR3 P4 P7 HC2
62 kD
49 kD
38 kD
ADA2
β-actin
D
HMDM SN
Serum
HC4i HC4ii HC6 HC1 HC1 HC3 P7
62 kD
49 kD
ADA2
E
HEK293T
EV WT R9W G47A G47R G47V N127Q T129P R169Q P344L W362R N370K del881 c.973 del1240
62 kD
49 kD
49 kD
WT G47R
WCE SN WCE SN
ADA2
β-actin

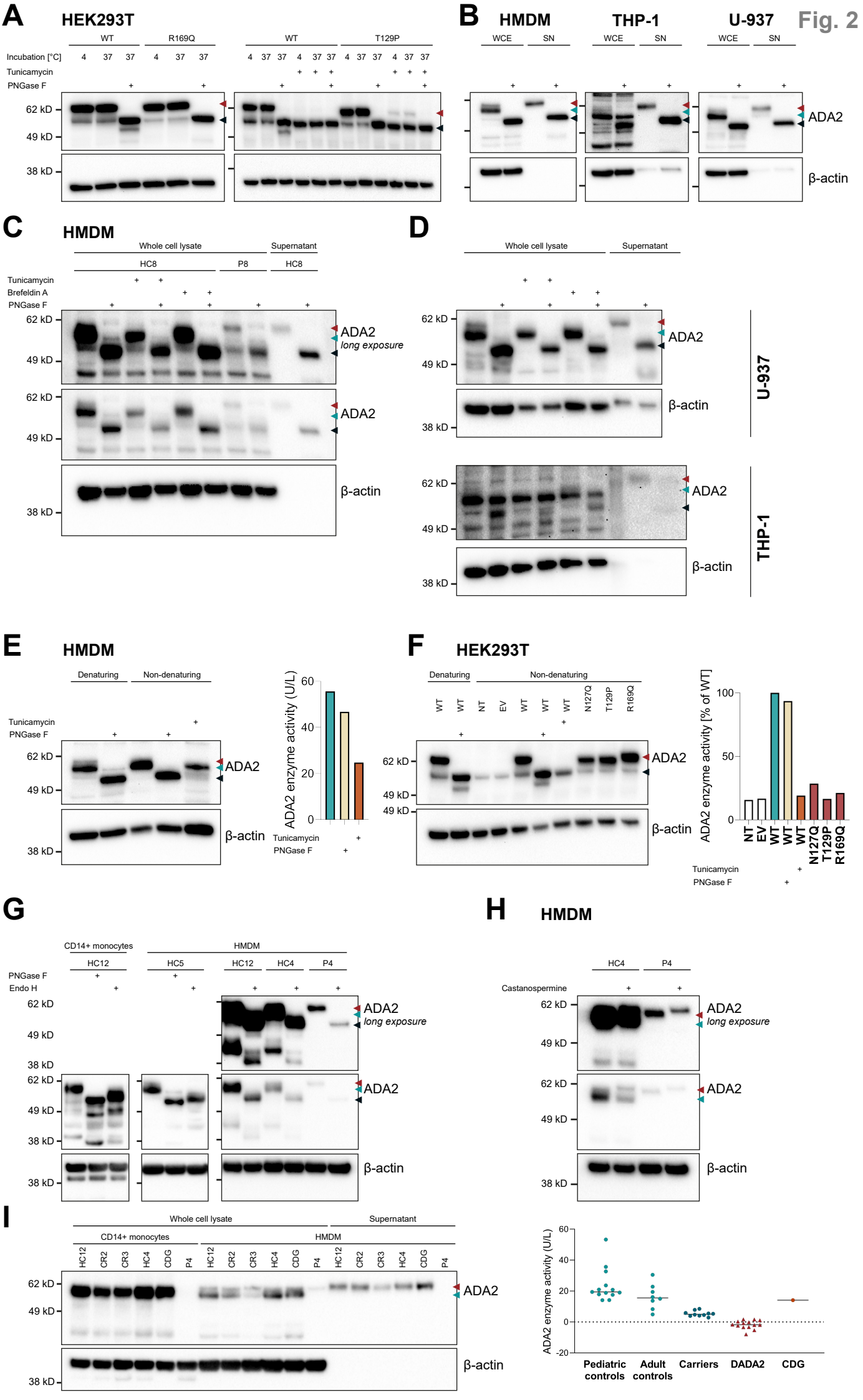

Fig. 2
A
HEK293T
WT
R169Q
WT
T129P
Incubation [°C]
Tunicamycin
PNGase F
62 kD
49 kD
38 kD
B
HMDM
THP-1
U-937
WCE
SN
ADA2
β-actin
C
HMDM
Whole cell lysate
Supernatant
HC8
P8
HC8
Tunicamycin
Brefeldin A
PNGase F
ADA2
long exposure
ADA2
β-actin
D
Whole cell lysate
Supernatant
ADA2
β-actin
U-937
THP-1
E
HMDM
Denaturing
Non-denaturing
Tunicamycin
PNGase F
ADA2
β-actin
ADA2 enzyme activity (U/L)
F
HEK293T
Denaturing
Non-denaturing
WT
WT
NT
EV
WT
WT
WT
N127Q
T129P
R169Q
ADA2
β-actin
ADA2 enzyme activity [% of WT]
NT
EV
WT
WT
WT
N127Q
T129P
R169Q
Tunicamycin
PNGase F
G
CD14+ monocytes
HMDM
HC12
HC5
HC12
HC4
P4
PNGase F
Endo H
ADA2
long exposure
ADA2
β-actin
H
HMDM
HC4
P4
Castanospermine
ADA2
long exposure
ADA2
β-actin
I
Whole cell lysate
Supernatant
CD14+ monocytes
HMDM
HC12
CR2
CR3
HC4
CDG
P4
ADA2
β-actin
ADA2 enzyme activity (U/L)
Pediatric controls
Adult controls
Carriers
DADA2
CDG

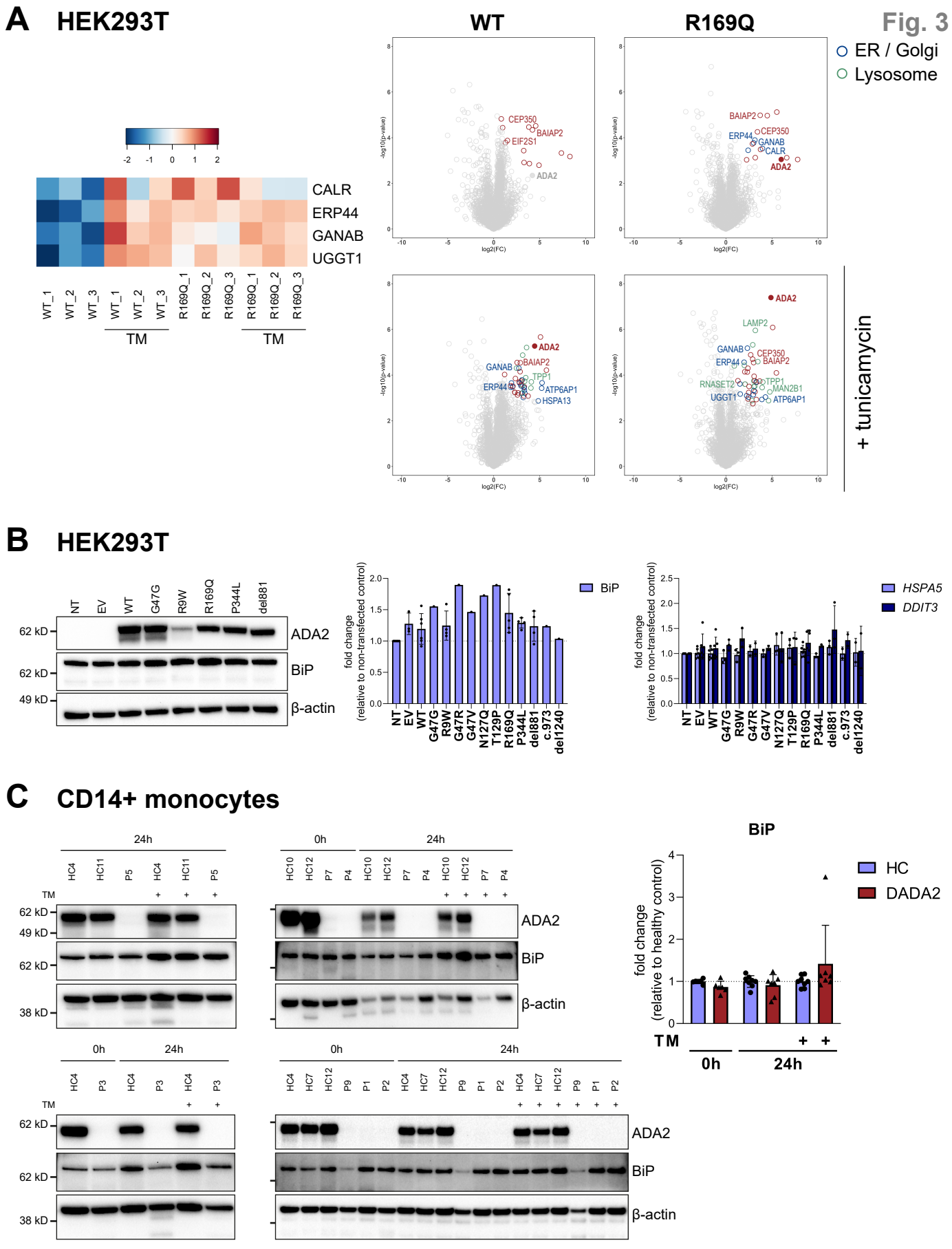

A
HEK293T
WT
R169Q
Fig. 3
ER / Golgi
Lysosome
CALR
ERP44
GANAB
UGGT1
WT_1
WT_2
WT_3
R169Q_1
R169Q_2
R169Q_3
TM
CEP350
BAIAP2
EIF2S1
ADA2
ERP44
GANAB
CALR
TPP1
ATP6AP1
HSPA13
LAMP2
RNASET2
MAN2B1
UGGT1
+ tunicamycin
log2(FC)
-log10(p-value)
B
HEK293T
NT
EV
WT
G47G
R9W
R169Q
P344L
del881
62 kD
49 kD
ADA2
BiP
β-actin
fold change
(relative to non-transfected control)
BiP
HSPA5
DDIT3
NT
EV
WT
G47G
R9W
G47R
G47V
N127Q
T129P
R169Q
P344L
del881
c.973
del1240
C
CD14+ monocytes
24h
0h
HC4
HC11
P5
HC10
HC12
P7
P4
P3
HC7
P9
P1
P2
TM
62 kD
49 kD
38 kD
ADA2
BiP
β-actin
BiP
HC
DADA2
fold change
(relative to healthy control)
TM
0h
24h

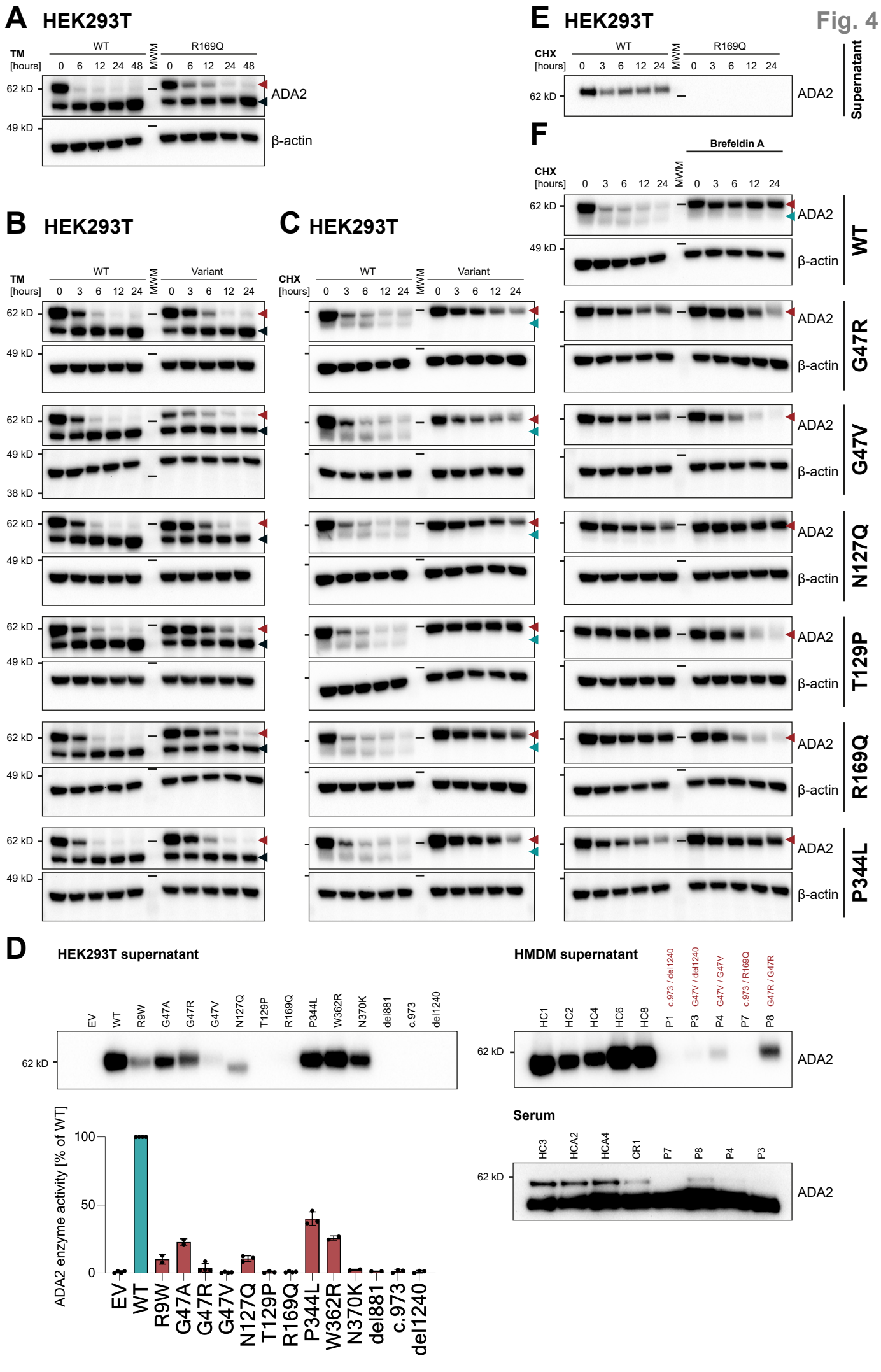
A HEK293T
TM [hours]
WT
MWM
R169Q
0 6 12 24 48
62 kD
49 kD
ADA2
β-actin
B HEK293T
TM [hours]
WT
MWM
Variant
0 3 6 12 24
38 kD
C HEK293T
CHX [hours]
D
HEK293T supernatant
EV WT R9W G47A G47R G47V N127Q T129P R169Q P344L W362R N370K del881 c.973 del1240
ADA2 enzyme activity [% of WT]
100
50
0
HMDM supernatant
HC1 HC2 HC4 HC6 HC8 P1 c.973 / del1240 P3 G47V / del1240 P4 G47V / G47V P7 c.973 / R169Q P8 G47R / G47R
Serum
HC3 HCA2 HCA4 CR1 P7 P8 P4 P3
E HEK293T
CHX [hours]
Supernatant
F
Brefeldin A
WT
G47R
G47V
N127Q
T129P
R169Q
P344L

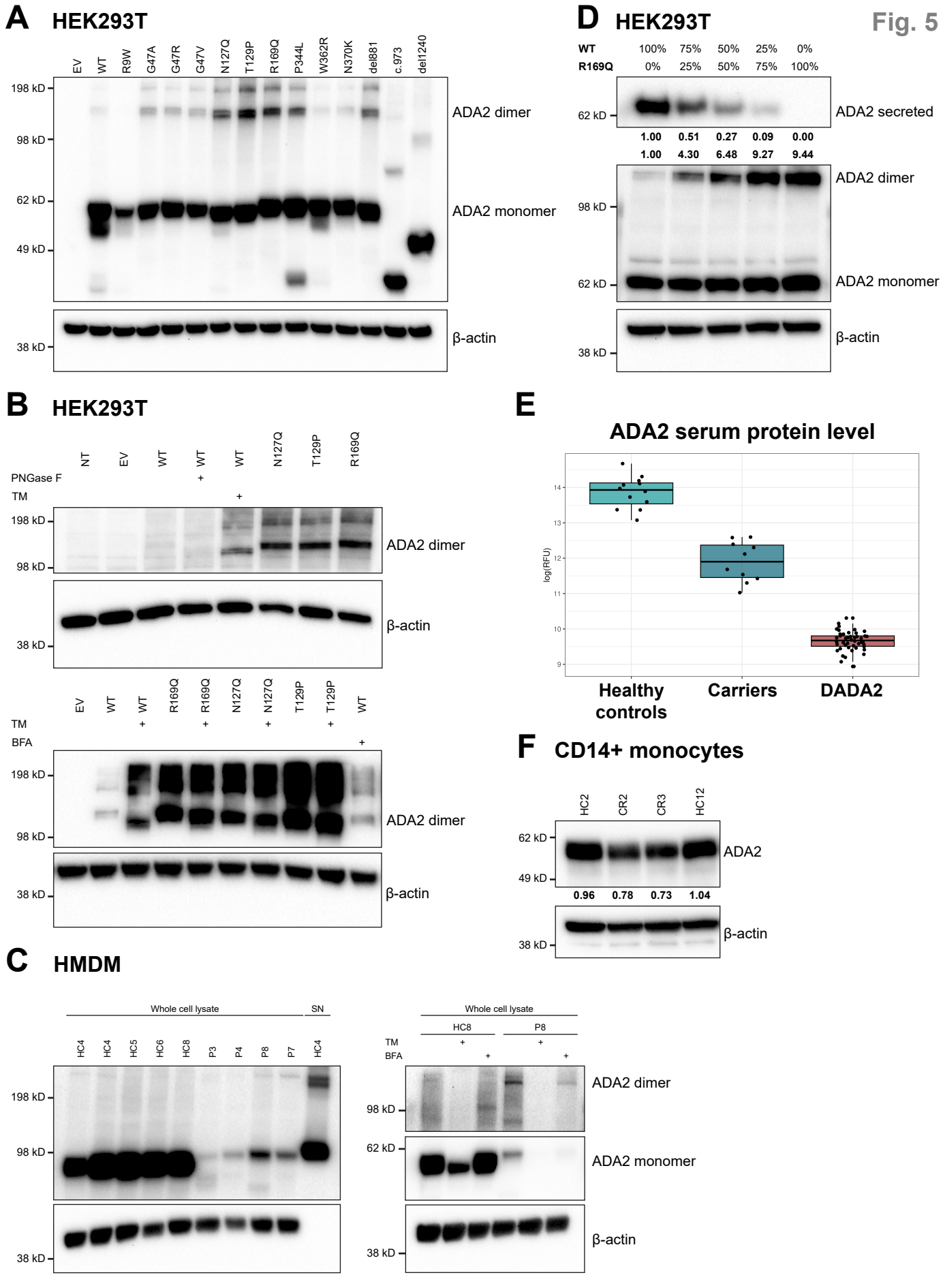

Fig. 5
A
HEK293T
EV
WT
R9W
G47A
G47R
G47V
N127Q
T129P
R169Q
P344L
W362R
N370K
del881
c.973
del1240
198 kD
98 kD
62 kD
49 kD
38 kD
ADA2 dimer
ADA2 monomer
β-actin
D
HEK293T
WT 100% 75% 50% 25% 0%
R169Q 0% 25% 50% 75% 100%
62 kD
ADA2 secreted
1.00 0.51 0.27 0.09 0.00
1.00 4.30 6.48 9.27 9.44
98 kD
62 kD
38 kD
ADA2 dimer
ADA2 monomer
β-actin
B
HEK293T
NT
EV
WT
WT
WT
N127Q
T129P
R169Q
PNGase F
TM
198 kD
98 kD
38 kD
ADA2 dimer
β-actin
EV
WT
WT
R169Q
R169Q
N127Q
N127Q
T129P
T129P
WT
TM
BFA
198 kD
98 kD
38 kD
ADA2 dimer
β-actin
E
ADA2 serum protein level
log(RFU)
14
13
12
11
10
9
Healthy controls
Carriers
DADA2
F
CD14+ monocytes
HC2
CR2
CR3
HC12
62 kD
49 kD
38 kD
ADA2
0.96 0.78 0.73 1.04
β-actin
C
HMDM
Whole cell lysate
SN
HC4
HC4
HC5
HC6
HC8
P3
P4
P8
P7
HC4
198 kD
98 kD
38 kD
Whole cell lysate
HC8
P8
TM
BFA
98 kD
62 kD
38 kD
ADA2 dimer
ADA2 monomer
β-actin

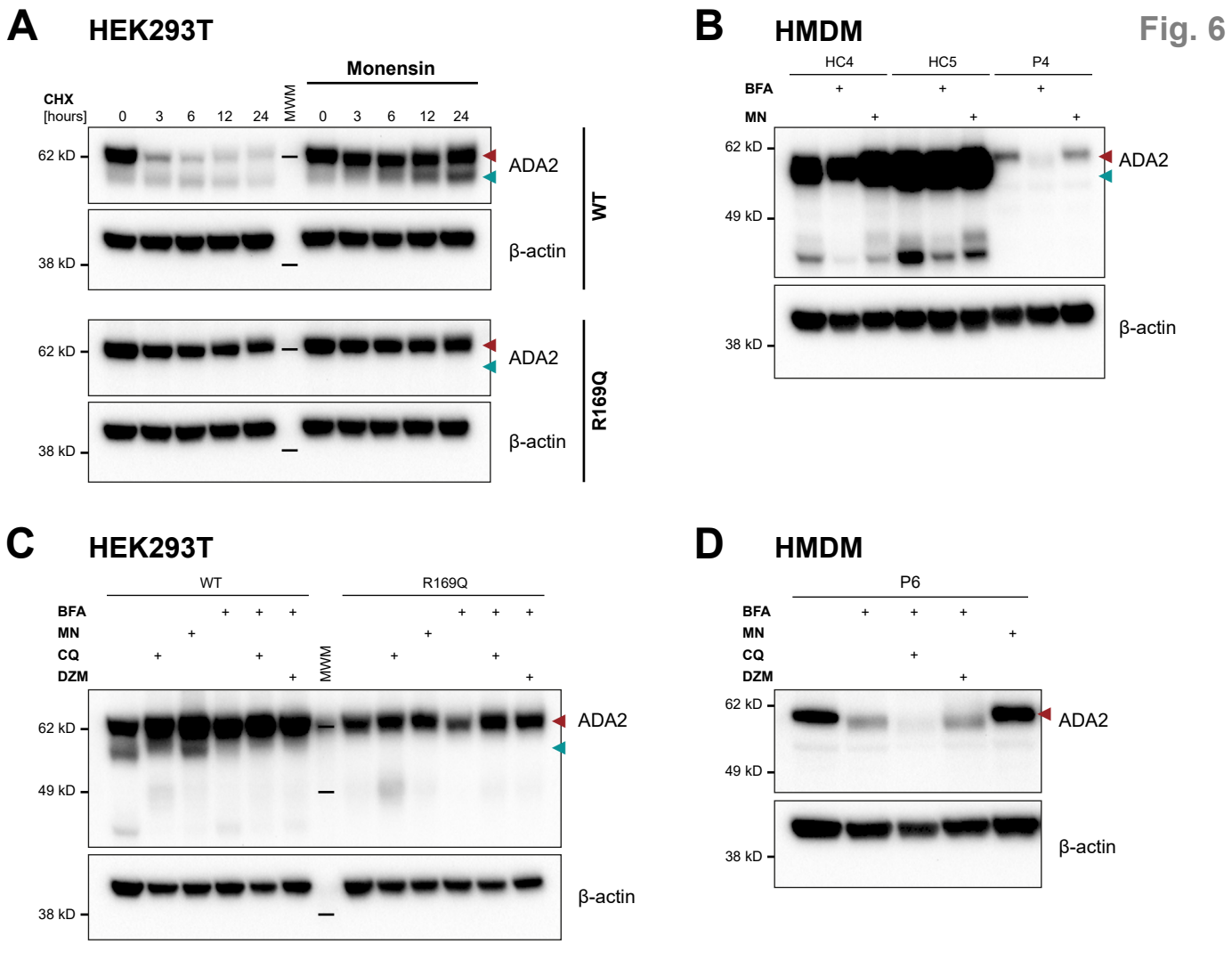
A
HEK293T
Monensin
CHX
[hours]
0
3
6
12
24
MWM
0
3
6
12
24
62 kD
38 kD
ADA2
β-actin
WT
R169Q
B
HMDM
HC4
HC5
P4
BFA
MN
62 kD
49 kD
38 kD
ADA2
β-actin
C
HEK293T
WT
R169Q
BFA
MN
CQ
DZM
MWM
62 kD
49 kD
38 kD
ADA2
β-actin
D
HMDM
P6
BFA
MN
CQ
DZM
62 kD
49 kD
38 kD
ADA2
β-actin

Tables

Table 1. Cohort characteristics

ID	Age [years]	Sex	Genotype	Predominant phenotype
P1	12	M	c.973-2A>G/c.del1240-1442 splice site (intron 6)/del exon 9	Vasculitis, hepatosplenomegaly, hypogammaglobulinemia
P2	14	F	c.973-2A>G/c.del1240-1442 splice site (intron 6)/del exon 9	Vasculitis, warts, hypogammaglobulinemia, arthralgia
P3	26	M	c.140G>T/c.del1240-1442 p.G47V/del exon 9	Bone marrow failure, hypogammaglobulinemia, hepatosplenomegaly
P4	26	M	c.140G>T/c.140G>T p.G47V/p.G47V	Hypogammaglobulinemia, hepatosplenomegaly
P5	6	F	c.140G>T/c.506G>A p.G47V/p.R169Q	Hypogammaglobulinemia, hepatosplenomegaly, stroke
P6	9	F	c.140G>T/c.506G>A p.G47V/p.R169Q	Bone marrow failure, hypogammaglobulinemia, hepatosplenomegaly
P7	32	F	c.973-2A>G/c.506G>A splice site (intron 6)/p.R169Q	Stroke, hypertension
P8	16	M	c.139G>A/c.139G>A p.G47R/p.G47R	Stroke, vasculitis
P9	10	F	c.973-2A>G/c.973-2A>G splice site (intron 6)/splice site (intron 6)	Vasculitis, hypogammaglobulinemia
P10	50	F	c.973-2A>G/c.506G>A splice site (intron 6)/p.R169Q	Vasculitis, leukopenia
CR1	39	F	WT/c. del1240-1442 WT/del exon 9	
CR2	38	F	WT/c.140G>T WT/p.G47V	
CR3	42	M	WT/c.506G>A WT/p.R169Q	